Incorporating multi-source uncertainties in fast building wall thermal resistance estimation through physics-based and multi-fidelity statistical learning models

H. Nasser, G. Perrin, R. Chakir, S. Demeyer, Julien Waeytens

Journal of Building Engineering 98 (2024) 111027

Contents lists available at ScienceDirect

Journal of Building Engineering

journal homepage: www.elsevier.com/locate/jobe

Incorporating multi-source uncertainties in fast building wall thermal resistance estimation through physics-based and multi-fidelity statistical learning models

H. Nasser [a,*], G. Perrin [a], R. Chakir [a], S. Demeyer [b], J. Waeytens [a]

[a] Université Gustave Eiffel, COSYS, IMSE, 77420 Champs-sur-Marne, France
[b] Laboratoire National de Métrologie et d'Essais, 78190 Trappes, France

ARTICLE INFO

Keywords:
Thermal resistance
Bayesian inference
Gaussian process regression
Multi-fidelity approach
Inverse problem

ABSTRACT

Meta-modelling and Bayesian inversion technique are proposed for fast and accurate *in-situ* estimation of the total thermal resistance (R_{Tot}) of walls using non-intrusive wall instrumentation. Various sources of uncertainties are taken into account to provide an enhanced credible interval for the thermal resistance estimate. In the considered protocol, a small zone of the internal surface of the wall is excited by a prototype to get faster *in situ* estimation and to limit the influence of external weather conditions. To be independent of the heat transfer coefficients and of the misknown layer thicknesses, which are difficult to estimate, we use herein the measurements of internal and external surface temperatures as boundary conditions in a thermal direct problem reformulated. A meta-model of the thermal model is created based on a statistical multi-fidelity approach with two levels of fidelity, Resistance-Capacitance (RC) and 1D models, to achieve the Bayesian estimation of the total thermal resistance in a reasonable computation time. The R_{Tot} estimation method is applied to realistic internal insulated walls (IIW), from poorly to highly insulated, under different weather conditions. Several numerical tests are carried out and credible intervals are provided to study the importance of the wall initial condition, the excitation time and the instrumentation. Finally, an experimental application is conducted using real measurements on an internal insulated wall (IIW) in Nancy (France). The obtained experimental results show that, in a short excitation time (10h) with a reduced instrumentation, the proposed method accurately estimates the minimum wall thermal resistance. For a standard wall of about 4 m^2 K/W, a relevant estimate of R_{Tot} with a relative deviation less than 10% can be achieved by using a polynomial initial temperature profile proposed in this study, sufficient measurements and an excitation time of 3 days. This study thus offers prospects for improved energy assessment of buildings before and after renovation.

1. Introduction

The building sector accounts for more than one third of the global energy consumption and it is expected to increase in the coming years [1,2]. In the European Union, this sector accounts for around 40% of the total energy consumption [3], and the implementation of good thermal insulation in buildings is considered as one of the main sources of energy savings. In France, a significant proportion of existing buildings (apartment blocks, houses, etc.) are particularly affected by energy losses and are

* Corresponding author.
E-mail addresses: hadi.nasser@univ-eiffel.fr (H. Nasser), guillaume.perrin@univ-eiffel.fr (G. Perrin), rachida.chakir@univ-eiffel.fr (R. Chakir), severine.demeyer@lne.fr (S. Demeyer), julien.waeytens@univ-eiffel.fr (J. Waeytens).

https://doi.org/10.1016/j.jobe.2024.111027
Received 12 July 2024; Received in revised form 20 September 2024; Accepted 10 October 2024
Available online 22 October 2024

therefore in need of renovation. To speed up this renovation process, the French thermal regulation RT2005 [4] imposed in 2005 an energy consumption target that resulted in a minimum resistance of 3 m^2 K/W for an opaque building wall. This value was revalued upwards in 2012 (RT2012) [5] to a minimum resistance of 4 m^2 K/W for new or renovated buildings. In 2020 [6], as a complement to RT2012, a switch from thermal to environmental regulations is applied, with the aim of reducing the carbon impact of buildings, further improving their energy performance and ensuring thermal comfort in scorching summers. In order to control these various stages of construction and renovation, an approach is needed to determine *in situ* the thermal resistance of a wall with associated credible interval.

In the literature, several existing studies propose approaches to identify the thermal properties of opaque walls. For example, in [7,8], the authors compare three approaches (deterministic and probabilistic) to identify the total resistance of walls using an active solicitation of the internal wall face. It is assumed that the thicknesses of each layer and the exchange coefficients are considered known. Authors take into account only the uncertainties of the measurements while other uncertainties may be present. They show that all three methods under controlled boundary conditions succeed numerically, in identifying the thermal resistance on an internal insulated wall for a total wall thicknesses less than 0.45 m, with 20% accuracy. Based on experiments carried out on a real wall in the laboratory, the authors explain that in a short time of measurement (10 h), only the first layers of the wall can be characterised in the proposed identification process. Another comparison of three methods (heat transfer matrix, analytical method and the finite element method) for determining wall thermal properties (conductivity and heat capacity) has been proposed by Sassine et al. [9]. These methods are based on five days of data in the random boundary conditions case and two days of data in the controlled case. The authors show that the results vary according to the method used and the boundary conditions, but remain satisfactory for the determination of the thermal properties studied. ISO 9869-1 [10] provides a simple method for determining thermal resistance from *in situ* measurements. However, due to its steady-state assumptions, this method can require long measurement periods and may be seasonally limited. Rasooli and Itard [11] have improved this method by adding instrumentation to reduce the measurement time and improve the accuracy of the results. Several methods [12–15] have been derived from ISO 8990 [16] (available only under laboratory conditions) and ISO 9869-1 [10] (dedicated to *in situ* measurements under specific environmental conditions), with ISO 9869-2 [17] extension, which involves long measurement times. A comparative study of five methods for determining thermal resistance was carried out by Deconinck and Roels [18]. The authors conclude that the reliability of methods for estimating thermal properties varies according to weather conditions. These properties are calculated according to the methods of EN ISO 13786 [19], used by Ricciu et al. [20] to determine the thermal properties of the layers of an experimental wall using a climatic chamber and harmonic loading. Similarly, Petojević et al. [21] used harmonic loading to determine the thermal properties of a multi-layer wall using thermal pulse response functions and a least squares estimator based on *in situ* experimental data. Although harmonic stresses give accurate results, they are mainly used in the laboratory. In the study [22], the authors propose a comparison between two modelling approaches, one based on a "white-box" model derived from the physical heat equation and the other on a "black-box" autoregressive exogeneous (ARX) model. The optimal parameter is estimated using the Levenberg–Marquardt algorithm [23,24], taking into account only the uncertainties of the measurement of the interior surface flux. They demonstrate that when the external temperature remains constant, both approaches provide accurate and similar estimates of the total thermal resistance. However, in other cases, only the "white-box" model-based approach manages to provide accurate estimates of the total thermal resistance. The study [25] proposes a deterministic identification of the thermal properties of wall bricks by individual characterisation of the materials. It provides reliable estimation results. A complement to this study is proposed in [26], it presents a laboratory identification of the thermophysical properties (thermal conductivity (λ) and capacity (ρC)) in masonry walls of building using the interior and exterior temperatures and fluxes of the wall. Assuming homogeneous material properties in the wall, the authors show that the identification of λ is done with good accuracy (error less than 15%) when considering a measurement time of more than 20 h. However, in the case of ρC the relative deviation exceeds 15% even for measurement time of up to 50 h. There are also several recent reviews on textitin-situ thermal evaluation methods. For example, Teni et al. [27] reviewed recent non-destructive *in-situ* methods for evaluating the thermal transmittance (U-value) of walls. Bienvenido-Huertas et al. [28] reviewed recent publications on wall U-value evaluation, but active evaluation methods and some basic theoretical models are lacking. Yang et al. [29] reviewed recent developments including steady-state methods, transient methods and other non-destructive evaluation methods. Fundamental theories as well as instrumentation and systems were analysed.

The vast majority of these methods can be described as deterministic, in the sense that most of the effort is focused on constructing a single deterministic estimator that is as accurate as possible. Many alternative studies take a Bayesian approach, which attempts to associate uncertainties and credible interval with these estimates. Among these methods, Biddulph et al. [30] developed a Bayesian estimation method to simultaneously estimate thermal resistance and effective thermal mass by comparing two simple wall models: a single thermal resistance model without thermal mass (NTM) and a two thermal resistance model with single thermal mass (STM). They showed that the STM model significantly reduces the time needed to thermally characterise the wall. This method was further improved by Gori et al. [31]. Another study [32] proposed a Bayesian approach to determine the thermal performance of a wall and the associated uncertainties. This approach was tested both on a virtual wall with known thermal properties and initial temperature, and on real data corresponding to 8 days of measurements. These different dynamic methods allowed the U-value to be determined, but still required several days of measurements. Based on a 1D model and assuming known layer thicknesses, an indirect determination of the thermal resistance was also applied in [33] on a IIW in climatic chamber (laboratory), while only taking into account temperature and flux measurement uncertainties in a Bayesian framework. The authors pointed out that the effect of uncertainties remains relatively small and cannot be fully interpreted in terms of bias with respect to a reference value, due to experimental limitations in quantifying this effect on the estimated thermal parameters. Another Bayesian approach based on experimental data collected over one year was proposed in [34] to estimate the thermal conductivity and time-varying

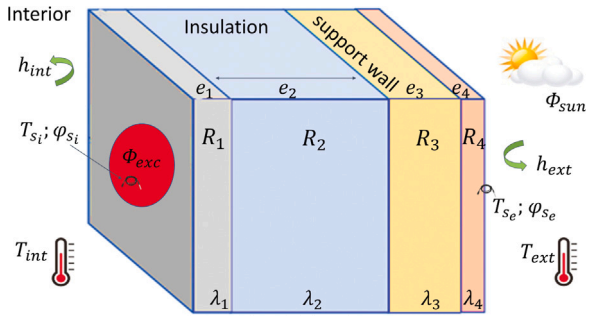

Fig. 1. Geometry of a 4-layer IIW considered in the study.

internal convective heat transfer coefficient of three layers of a wall. Despite its high computational cost (about 10^5 direct model computations), this method provides parameter estimates with low standard deviation.

Most of previous works has focused on the estimation of wall thermal resistance under laboratory conditions or using deterministic approaches or considering simplified assumptions in Bayesian formalism. The aim of this study is to better take into account the various sources of uncertainty and to provide a fast *in-situ* identification of the thermal resistance of walls with its associated credibility interval using Bayesian framework. The consideration of the various sources of uncertainty makes it easier to interpret the estimation results, and in particular the main causes of the uncertainties obtained (thus facilitating the path to potential improvements). In this work, the estimation of the thermal resistance of a wall is formulated as an inverse problem. The proposed method allows not only the determination of the total thermal resistance of the wall, but also the resistances of each individual layer. Using a meta-model constructed from physical thermal numerical models and a multi-fidelity statistical approach, we therefore search the most likely thermal properties of the wall to lead to such thermal measured responses. The specificity of this work is to develop a method which is at the same time operational, robust, and explainable. By operational, we mean a method that is fast, not very intrusive from an experimental point of view and easily deployable on building walls. It requires only very partial information on the wall to be studied (only the number of layers of the wall will be required), while being relatively cheap numerically. By robust, we mean that the method is capable of estimating with good accuracy the insulation properties of a large number of walls with very different properties (from poorly to highly insulated walls), while being relatively independent of the climatic conditions prevailing during the experiment.

The articulation of this paper is thus divided into three main parts. Section 2 first presents the thermal direct numerical model on which the inversion problem will be based. The multi-fidelity predictors and Bayesian approach proposed for estimating the thermal properties of the wall are then the subject of Section 3. Section 4 finally presents the efficiency of the proposed method to estimate the thermal properties of very different walls, when confronted to very different weather conditions. These applications will first be carried out on simulated data, in order to be able to more easily highlight the strengths and limits of the proposed approach in a perfectly controlled framework, then in a second step on experimental data on a real internal insulated wall in natural weather conditions.

2. Problem statement and thermal direct modelling

In this section, the direct model that will be used to estimate the thermal properties of a wall is presented. Firstly, we introduce the structure of internal insulated wall (IIW) and the notations that will be used throughout the article. IIW is widespread in new building construction in France. In renovation actions, the advantage of IIW is that it is often less expensive than external insulation and has no impact on the external appearance of the building, which can be regulated by urban planning. Let us note that the proposed methodology can also be adapted and applied to many other wall types. In particular, we will discuss the influence of the heat transfer coefficients and how the thermal problem can be rewritten to get rid of this influence, as well as the influence of the initial condition.

2.1. Wall structures, properties and introduction to the identification problem

In this work, we mainly focus on IIW as presented in Fig. 1. Such a wall is composed of four layers, with different physical properties. Let t be the time. For each layer $i \in \{1,2,3,4\}$, we note λ_i (W/(m K)) the thermal conductivity, ρC_i (J K^{-1}/m^3) the volumetric heat capacity, e_i (m) the thickness, and $R_i = e_i/\lambda_i$ (m^2 K/W) the associated thermal resistance (see Fig. 1 for a graphic visualisation of these quantities).

All these quantities are supposed unknown. Only relatively large value ranges derived from expert knowledge are available. To verify that the wall complies with the thermal insulation performance specified in building regulations such as in [6], our main goal in this article is to identify *in-situ*, the total thermal resistance of the wall,

$$R_{\text{Tot}} = R_1 + R_2 + R_3 + R_4.$$

As it was proposed in [7], an active thermal solicitation is considered, which consists in heating a zone on the inner surface of the wall with a Heaviside-type excitation as presented in red in Fig. 1. As the objective is not to qualify thermal bridges, the thermal excitation must not be placed near windows, doors or corners of the room. Moreover, for easy installation by an operator, the heating device must not be cumbersome and must be placed on the interior surface of the wall. For more details on the experimental prototype developed, see [7,8]. Compared to standardised methods [10], this controlled excitation allows a faster identification of R_{Tot} (in particular R_2, which is the main contributor to the total resistance), while overcoming the limitations associated with sensitivities to external conditions [22]. Once the excitation starts, the heat flux excitation on the internal wall surface, denoted $\boldsymbol{\Phi}_{\text{exc}}$, increases to reach a maximum of approximately 400 W/m^2. The inside and outside temperatures of the air are respectively denoted by T_{int} and T_{ext}. In natural weather conditions, the external surface of the wall is moreover exposed to a solar flux, which is noted $\boldsymbol{\Phi}_{\text{sun}}$ and which varies over time, and we denote by h_{int} (respectively h_{ext}) the interior (respectively exterior) coefficient of heat transfer. For operational purposes, the measurement in existing buildings must be done in non-intrusive and non-destructive ways. Hence, a surface temperature sensor and a thermal flux sensor are placed at the centre of the heating zone on the inner surface of the wall. Two sensors can be added to the outer surface of the wall to measure the outer surface temperature and outer thermal flux. The surface temperatures (resp. the thermal fluxes) are denoted T_{S_i} and T_{S_e} (resp. $\varphi_{\text{S}_\text{i}}$ and $\varphi_{\text{S}_\text{e}}$). The subscript S_i refers to the interior surface, while S_e refers to the exterior surface of the wall. At last, we note T_{W_0} the temperature at any position of the wall at the initial time of the experiment.

Among all these quantities, it is important to make a distinction between the quantities that :

- We assume to know from measurements : $T_{\text{ext}}, T_{\text{int}}, T_{\text{S}_\text{i}}, T_{\text{S}_\text{e}}, \varphi_{\text{S}_\text{i}}, \varphi_{\text{S}_\text{e}}$,
- It is possible to know by installing a more or less sophisticated measuring device : $\boldsymbol{\Phi}_{\text{sun}}, \boldsymbol{\Phi}_{\text{exc}}$,
- We assume unknown : $e_i, \rho C_i, R_i, T_{\text{W}_0}, h_{\text{int}}, h_{\text{ext}}$.

2.2. Influence of the global exchange coefficients

It is well known that the internal (h_{int}) and external (h_{ext}) heat transfer coefficients have a strong impact on T_{S_i}, T_{S_e}, $\varphi_{\text{S}_\text{i}}$ and $\varphi_{\text{S}_\text{e}}$ [35]. As these measured quantities are used to estimate the thermal properties of the wall, it seems essential to be able to identify the internal and external heat exchange coefficients h_{int}, h_{ext} or to limit the influence of these coefficients. On the one hand, optical measurements or infrared temperature mapping methods can be used to estimate h_{int} and h_{ext}. But they generally require expensive equipment that do not fulfil the objective of our work [36–38]. On the other hand, they can be estimated, at the same time as the other properties of the wall. However, as these quantities vary according to the weather conditions (air flow, temperature, etc.), it greatly complicates the estimation problem.

Therefore, to avoid estimating these coefficients (which is not the aim of the study), a reformulation of the thermal problem independent of h_{int} and h_{ext} is proposed in Section 2.3, which consists in imposing T_{S_i} and T_{S_e} as boundary conditions (see Eq. (4)), and make the inversion problem rely on $\varphi_{\text{S}_\text{i}}$ and $\varphi_{\text{S}_\text{e}}$ only. Note that in this case, the estimation problem does not need the measurement of $\boldsymbol{\Phi}_{\text{sun}}$ and $\boldsymbol{\Phi}_{\text{exc}}$. The measurement of T_{int} and T_{ext} is also not required.

2.3. One-dimensional reformulated thermal model

The 3D thermal model appears to be too expensive numerically to be directly used in a Bayesian formalism for the estimation of the total thermal resistance of a wall. We therefore propose to consider a simple 1D model in the inversion process. Since the thicknesses of each layer is not known, we propose to scale the thermal equations so that they no longer depend on e_i by making a change of variable. If $x \in [0, e_1 + e_2 + e_3 + e_4]$ characterises the position in the wall, we note $x_i \in [0,1]$ the normalised depth in layer i, such that : $x_1 = x/e_1$ for $x \in [0, e_1]$, $x_i = (x - \sum_{j=1}^{i-1} e_j)/e_i$ for $x \in \left[\sum_{j=1}^{i-1} e_j\,,\ \sum_{j=1}^{i} e_j\right]$. As a consequence, the 1D model only depends on the thermal resistances R_i and the product of the thicknesses and volumetric heat capacities $e_i \times \rho C_i$ in each layer i, that will be designated in the following as layer capacitance, and will be grouped in a single parameter noted $e\rho C_i$ to reduce the number of unknowns. But we also prevent ourselves from precisely identifying the ρC_i of the wall (we will only know them up to the thickness of the wall). For all $1 \le i \le 4$, let $T_i(x_i, t)$ be the temperature in layer i at depth $x_i \in [0,1]$ and time $t \in [t_0, t_f]$. The constants t_0 and t_f therefore correspond to the initial and final times of the experiment. The scaled partial differential equation that T_i must satisfy at all x_i and all t is therefore given by

$$e\rho C_i \frac{\partial T_i}{\partial t} - \frac{1}{R_i}\frac{\partial^2 T_i}{\partial {x_i}^2} = 0, \quad 1 \le i \le 4. \tag{1}$$

The following continuity conditions (of temperature and flux) at the different layer interfaces and at any time $t \in [t_0, t_f]$ must also be ensured:

$$T_i(x_i = 1, t) = T_{i+1}(x_{i+1} = 0, t), \quad 1 \le i \le 3, \tag{2}$$

$$\frac{1}{R_i}\frac{\partial T_i}{\partial x_i}(x_i = 1, t) = \frac{1}{R_{i+1}}\frac{\partial T_{i+1}}{\partial x_{i+1}}(x_{i+1} = 0, t), \quad 1 \le i \le 3. \tag{3}$$

At last, we define boundary conditions (at the inner and outer surfaces of the wall, i.e. at $x_1 = 0$ and $x_4 = 1$) and initial condition:

$$T_1(x_1 = 0, t) = T_{S_i}(t), \quad T_4(x_4 = 1, t) = T_{S_e}(t), \tag{4}$$

$$T_i(x_i, t = t_0) = T_{W_0}(x_i), \quad x_i \in [0, 1], \quad 1 \leq i \leq 4, \tag{5}$$

Let us notice that T_{S_i}, T_{S_e}, φ_{S_i}, and φ_{S_e}, can now be written:

$$T_{S_i} = \left\{T_1(x_1 = 0, t),\ t \in [t_0, t_f]\right\}, \quad T_{S_e} = \left\{T_4(x_4 = 1, t),\ t \in [t_0, t_f]\right\}, \tag{6}$$

$$\varphi_{S_i} = \left\{-\frac{1}{R_1}\frac{\partial T_1}{\partial x_1}(x_1 = 0, t),\ t \in [t_0, t_f]\right\}, \quad \varphi_{S_e} = \left\{-\frac{1}{R_4}\frac{\partial T_4}{\partial x_4}(x_4 = 1, t),\ t \in [t_0, t_f]\right\}. \tag{7}$$

2.4. Influence of the initial condition (IC)

In general, it is not straightforward to know the initial temperature in the wall (T_{W_0}). In the literature, many studies conducted in laboratories generally assume that the initial temperature in the wall (or the layers) is known at $t = t_0$, as it is done in [22,34,35]. For experiments that are conducted *in situ* under not necessarily controlled conditions, the initial temperature in the wall is most of the time calculated based on stationary assumption, as it is done in [7]. However, as it will be illustrated in the application section, this assumption of stationary is often invalid, and can strongly degrade the quality of the estimation of the thermal proprieties of the wall studied. To reduce the influence of the initial condition on the identification of R_{Tot}, two ways of improvement are thus proposed herein. When possible, before the estimation procedure, we recommend using a stabilisation period during which the heat flux excitation on indoor wall face Φ_{exc} is fixed at 0 W/m^2. The longer this stabilisation period, the less important the initial temperature in the wall will be. From the analysis of a large number of numerical tests and in agreement with [39], we noticed that imposing a stabilisation period of 3 days made it possible to almost overcome this lack of knowledge about the wall initial temperature. If it is not possible to achieve this long stabilisation period, we propose to replace the stationary hypothesis by an hypothesis of piece-wise polynomial evolution of the temperature in the wall, and to estimate the coefficients of these polynomials from the measurements of the temperatures and the surface fluxes on wall faces at $t = t_0$ only. The proposed temperature profiles are therefore chosen as first-order polynomials for the temperatures in layers 1 and 2 (internal coating and insulation), and second-order polynomials for the temperatures in layers 3 and 4 (support wall and external coating):

$$\begin{cases} T_{i_0}(x_i, t = t_0) = a_i x_i + b_i, & i \in \{1, 2\}, \\ T_{i_0}(x_i, t = t_0) = a_i x_i^2 + b_i x_i + c_i, & i \in \{3, 4\}. \end{cases} \tag{8}$$

We denote by T_W^{Poly} this polynomial approximation of the true initial temperature T_{W_0} in the wall at the initial time. This choice is on the one hand motivated by the fact that there is more variation on the exterior side (temperature and solar flux), and on the other hand by the fact that the conditions of continuity in temperature and flux and the measured temperatures and heat fluxes on indoor and outdoor wall faces only allow us to estimate 10 coefficients for these profiles (two equations for each of the five interfaces for a 4-layer wall). After testing the proposed profiles on IIW and comparing with other possible configuration profiles, it appear to be a very interesting choice in our application.

For the sake of concision, the details of the estimation of these coefficients are presented in Appendix A.

2.5. Thermal direct model and set parameters

As mentioned above, the aim of this study is to identify the unknown thermal properties of the walls under investigation, in particular the total thermal resistance. Fig. 2 illustrates the two main phases of the test: the stabilisation phase (between t_0^S and t_0) and the excitation phase (between t_0 and t_f). Only the measurements taken during the excitation phase are used in the identification procedure. The surface temperature measurements (T_{S_i} and T_{S_e}) and the temperature T_{W_0} in the wall at $t = t_0$ are used as boundary conditions and initial condition respectively in the thermal model. The heat flux measurements φ_{S_i} and φ_{S_e} are used in the inverse problem to estimate the thermal resistances (R_i) and the capacitance ($e\rho C_i$) of the four layers. To facilitate the reading, all the parameters to be estimated are grouped together in the vector

$$\boldsymbol{z} = (R_1, R_2, R_3, R_4, e\rho C_1, e\rho C_2, e\rho C_3, e\rho C_4). \tag{9}$$

Thanks to this formulation, it can be noted that the thermal model is no longer dependent of the indoor and outdoor temperatures (T_{int}, T_{ext}), of the exchange coefficients (h_{int}, h_{ext}), nor of the solar and excitation fluxes (Φ_{sun}, Φ_{exc}). In this way, the model only depends on measurable or controllable quantities, to make it as easy as possible to estimate the parameters related to the wall's resistance and thermal capacitance.

3. Bayesian estimation of the total thermal resistance of internal insulated walls

In this section, the proposed method to identify the thermal resistance of a multi-layer wall is presented. The Bayesian formulation is presented in Section 3.1. In order to reduce the numerical costs associated with the estimation, we then explain in Section 3.2.3 how to couple this previous formulation to statistical learning methods. Finally, an analysis of the sources of uncertainty is presented in Section 3.2.

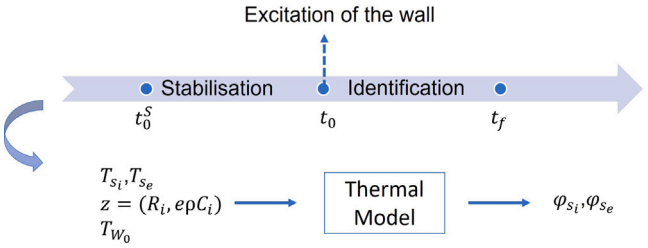

Fig. 2. Graphical representation of the direct model used for the parameter estimation.

3.1. Bayesian formalism

The objective of this work is to estimate the vector $\boldsymbol{z}$ that characterises the thermal properties of a four-layers wall. To incorporate the various sources of uncertainty in the problem, a Bayesian approach is adopted in this work [40]. This approach models the unknown quantities as random variables: the vector $\boldsymbol{z}$ to be estimated and the different errors that may affect the measurements and/or the model response are therefore modelled by random vectors. In this context, estimating $\boldsymbol{z}$ no longer means searching for a single deterministic value, but requires characterising its *a posteriori* probability distribution, conditioned by the various measured quantities of the problem. The information provided by such a Bayesian inversion approach is therefore richer, in the sense that the *a posteriori* distribution quantifies the accuracy of the estimate in a natural way: the wider the domain over which this *a posteriori* law is spread, the less relevant the estimate, and vice versa. We denote by $\pi(\boldsymbol{z})$ the *a priori* probability density function (PDF) of $\boldsymbol{z}$, which we will consider to be uniform over a well-chosen domain of definition $\Omega \subset \mathbb{R}^8$ using expert knowledge (see [41] for more details about expert elicitation). The choice of the *a priori* knowledge is a central step in the proposed Bayesian approach. It must be chosen so that the reference value to be estimated lies within the interval of the *a priori* distribution. In other words, if the *a priori* interval is too small and does not contain the reference, the method will not be able to find the correct value, but will return the value in the interval in question that are most compatible with the measurements available. The *a posteriori* distribution, noted $\pi(\boldsymbol{z}|\boldsymbol{y}^{\text{mes}})$, can then be written from the Bayes' formula under the form

$$\pi(\boldsymbol{z}|\boldsymbol{y}^{\text{mes}}) = \frac{\pi(\boldsymbol{z}) \times \pi(\boldsymbol{y}^{\text{mes}}|\boldsymbol{z})}{\int_{\boldsymbol{z}'} \pi(\boldsymbol{z}') \times \pi(\boldsymbol{y}^{\text{mes}}|\boldsymbol{z}') d\boldsymbol{z}'}, \quad \boldsymbol{z} \in \Omega, \tag{10}$$

where the symbol | is for statistical conditioning, $\pi(\boldsymbol{y}^{\text{mes}}|\boldsymbol{z})$ is the likelihood function, and $\boldsymbol{y}^{\text{mes}}$ gathers the measured values of $\varphi_{\text{S}_\text{i}}$ and $\varphi_{\text{S}_\text{e}}$ at N_t different times between t_0 and t_f, which we propose to note $t_1, \dots, t_{\text{N}_\text{t}}$. We note $N_t^{\max}$ the dimension of y^{mes}, which is equal to $2N_t$ when the measurements of $\varphi_{\text{S}_\text{i}}$ and $\varphi_{\text{S}_\text{e}}$ are available, and to N_t if only the measurements of $\varphi_{\text{S}_\text{i}}$ are available.

The estimation of $\boldsymbol{z}$ therefore requires the introduction of the likelihood function $\boldsymbol{z} \mapsto \pi(\boldsymbol{y}^{\text{mes}}|\boldsymbol{z})$, which is supposed to link the thermal characteristics of the wall to the measurements collected. In order to construct this likelihood function, we introduce several notations associated to the heat fluxes $\varphi_{\text{S}_\text{i}}$ and $\varphi_{\text{S}_\text{e}}$. We first note $\boldsymbol{y}$ the vector gathering the true (but unknown) values of $\varphi_{\text{S}_\text{i}}$ and $\varphi_{\text{S}_\text{e}}$ at the different discretisation times, such that

$$\boldsymbol{y}^{\text{mes}} = \boldsymbol{y} + \varepsilon_{\varphi}^{\text{mes}}, \tag{11}$$

where $\varepsilon_{\varphi}^{\text{mes}}$ is the measurement error (whose properties depend on the sensors used). We then assume that $\boldsymbol{y}$ can be approximated with accuracy by a 3D thermal model of the wall, when considering the true boundary condition temperatures on the interior and exterior surfaces (T_{S_i} and T_{S_e}) and the true initial temperature in the wall at the initial time t_0 (T_{W_0}).

As explained in Section 2.3, the time required to solve such 3D models being significant, we propose to limit ourselves to the use of a 1D thermal model for the estimation step. We thus denote by $\boldsymbol{u}^{\text{1D}}(\boldsymbol{z}; T_{\text{S}_\text{i}}, T_{\text{S}_\text{e}}, T_{\text{W}_0})$ the approximation of $\boldsymbol{y}$ using the 1D thermal model introduced in Section 2.3. The three true temperature fields $T_{\text{S}_\text{i}}, T_{\text{S}_\text{e}}, T_{\text{W}_0}$ are however unknown. Concerning T_{S_i} and T_{S_e}, we only have access to noisy measurements of these temperatures. Two additional approximations are then introduced to approximate this link between the vector of measurements $\boldsymbol{y}^{\text{mes}}$ and the outputs of the 1D code. We first propose to replace T_{S_i} and T_{S_e} by smoothed versions noted $T_{\text{S}_\text{i}}^{\text{Smooth}}$ and $T_{\text{S}_\text{e}}^{\text{Smooth}}$ (see Section 3.2.2 for more details). Then, we propose to replace the true initial temperature in the wall T_{W_0} by the initial temperature $T_{\text{w}}^{\text{Poly}}$ that is derived from a polynomial approximation as explained in Section 2.4. Finally, to reduce the numerical cost of the 1D model in the Bayesian inversion procedure, we propose to replace the function $\boldsymbol{z} \mapsto \boldsymbol{u}^{\text{1D}}(\boldsymbol{z}; T_{\text{S}_\text{i}}^{\text{Smooth}}, T_{\text{S}_\text{e}}^{\text{Smooth}}, T_{\text{w}}^{\text{Poly}})$ by a multi-fidelity meta-model $\boldsymbol{z} \mapsto \boldsymbol{u}^{\text{Meta}}(\boldsymbol{z}; T_{\text{S}_\text{i}}^{\text{Smooth}}, T_{\text{S}_\text{e}}^{\text{Smooth}}, T_{\text{w}}^{\text{Poly}})$, that is to say a cheap-to-evaluate mathematical approximation of this function (the details of this last approximation are provided in Section 3.2.3). Naturally, replacing the 3D model with a 1D meta-model, and replacing the temperatures $T_{\text{S}_\text{i}}, T_{\text{S}_\text{e}}$ and T_{W_0} with approximate versions, is likely to introduce new errors into the problem. The link between $\boldsymbol{y}^{\text{mes}}$ and $\boldsymbol{u}^{\text{Meta}}(\boldsymbol{z}; T_{\text{S}_\text{i}}^{\text{Smooth}}, T_{\text{S}_\text{e}}^{\text{Smooth}}, T_{\text{w}}^{\text{Poly}})$ is thus written in the new form:

$$\boldsymbol{y} = \boldsymbol{u}^{\text{Meta}}(\boldsymbol{z}; T_{\text{S}_\text{i}}^{\text{Smooth}}, T_{\text{S}_\text{e}}^{\text{Smooth}}, T_{\text{w}}^{\text{Poly}}) + \varepsilon_{\varphi}^{\text{mes}} + \varepsilon_{\text{T}}^{\text{mes}} + \varepsilon^{\text{Meta}} + \varepsilon^{\text{Res}}, \tag{12}$$

where $\varepsilon_T^{\text{mes}}$ is associated with the replacement of $(T_{\text{S}_\text{i}}, T_{\text{S}_\text{e}})$ by $(T_{\text{S}_\text{i}}^{\text{Smooth}}, T_{\text{S}_\text{e}}^{\text{Smooth}})$, $\varepsilon^{\text{Meta}}$ corresponds to the error due to the approximation of the 1D model by a meta-model, and ε^{Res} takes into account the modelling error associated with the replacement of the 3D

model with a 1D model, as well as any other residual errors that may be present (these potential residual errors will be explained later in Section 3.2.4).

Even if this complicates the expressions, decomposing the difference between $\boldsymbol{y}^{\text{mes}}$ and $\boldsymbol{u}^{\text{Meta}}(\boldsymbol{z}; T_{\text{S}_\text{i}}^{\text{Smooth}}, T_{\text{S}_\text{e}}^{\text{Smooth}}, T_{\text{w}}^{\text{Poly}})$ into four error terms is motivated by a concern for physical interpretability of the results, to which we will return in Section 3.2. These different errors are indeed associated with different phenomena, on which it could be possible to work independently (by changing the measuring device, or by considering more sophisticated physical models for example). For the sake of simplicity, the prediction provided by the meta-model, $\boldsymbol{u}^{\text{Meta}}(\boldsymbol{z}; T_{\text{S}_\text{i}}^{\text{Smooth}}, T_{\text{S}_\text{e}}^{\text{Smooth}}, T_{\text{w}}^{\text{Poly}})$, will be written $\boldsymbol{u}^{\text{Meta}}(\boldsymbol{z})$ in the following, and we model the four errors in the form of Gaussian vectors that are centred and independent of each other. Let $\boldsymbol{\Sigma}_\varphi$, $\boldsymbol{\Sigma}_T$, $\boldsymbol{\Sigma}_{\text{meta}}(\boldsymbol{z})$ and $\boldsymbol{\Sigma}_{\text{res}}$ be the covariance matrices of $\varepsilon_\varphi^{\text{mes}}$, $\varepsilon_T^{\text{mes}}$, $\varepsilon^{\text{Meta}}$, and ε^{Res} respectively, whose definition will be detailed in Section 3.2. By denoting $\boldsymbol{W}(\boldsymbol{z})$ the sum of these four covariance matrices ($\boldsymbol{W}(\boldsymbol{z}) = \boldsymbol{\Sigma}_\varphi + \boldsymbol{\Sigma}_T + \boldsymbol{\Sigma}_{\text{meta}}(\boldsymbol{z}) + \boldsymbol{\Sigma}_{\text{res}}$), the likelihood function is finally written

$$\pi(\boldsymbol{y}^{\text{mes}}|\boldsymbol{z}) = \frac{\exp\left(-\frac{1}{2}\left(\boldsymbol{y}^{\text{mes}} - \boldsymbol{u}^{\text{Meta}}(\boldsymbol{z})\right)^T \boldsymbol{W}(\boldsymbol{z})^{-1}\left(\boldsymbol{y}^{\text{mes}} - \boldsymbol{u}^{\text{Meta}}(\boldsymbol{z})\right)\right)}{\sqrt{(2\pi)^{N_t^{\max}} \det(\boldsymbol{W}(\boldsymbol{z}))}}, \quad \boldsymbol{z} \in \Omega. \tag{13}$$

where $(.)^{-1}$ (respectively det) the inverse (respectively the determinant) of the matrix.

Since the denominator in Eq. (10) is unknown, we use a Markov Chain Monte Carlo (MCMC) approach [42,43] to generate a sequence of N_s values of $\boldsymbol{z}$, denoted $\{\boldsymbol{z}^1, \dots, \boldsymbol{z}^{N_s}\}$, which can be considered as independent realisations of a random vector of PDF $\pi(\boldsymbol{z}|\boldsymbol{y}^{\text{mes}})$. To explore the posterior distribution, we focus in this work on the Metropolis–Hastings (MH) algorithm [44,45], whose principle is summarised in Appendix B. Finally, it is possible to post-process these N_s values of $\boldsymbol{z}$, in order to deduce the most likely value of $\boldsymbol{z}$, which we denote by $\boldsymbol{z}^{\text{MAP}}$, and which is defined by:

$$\boldsymbol{z}^{\text{MAP}} \in \arg\max_{1 \le i \le N_s} \pi(\boldsymbol{z}^i) \times \pi(\boldsymbol{y}^{\text{mes}}|\boldsymbol{z}^i), \tag{14}$$

but also credible intervals of level $\alpha \in (0,1)$ for each component z_i of $\boldsymbol{z}$, noted $CI_i(\alpha)$ and defined as the interval of minimum length such that

$$\int_{CI_i(\alpha)} \pi(z_i|\boldsymbol{y}^{\text{mes}}) dz_i = \alpha, \tag{15}$$

where $\pi(z_i|\boldsymbol{y}^{\text{mes}})$ is the PDF of z_i conditioned by the observations gathered in $\boldsymbol{y}^{\text{mes}}$, which can be approximated from $\{\boldsymbol{z}^1, \dots, \boldsymbol{z}^{N_s}\}$ using kernel methods for instance (see [46] for more details about this sample-based PDF reconstruction).

3.2. Description of errors and quantification of uncertainties

According to Eq. (12), the measure $\boldsymbol{y}^{\text{mes}}$ is expressed as the sum of a meta-model-based prediction and four error terms, which we propose to explore in more detail in this section.

3.2.1. Measurement error associated with the measured fluxes

The first error term, $\varepsilon_\varphi^{\text{mes}}$, is the measurement error of the fluxes on the interior and exterior wall surfaces ($\varphi_{\text{S}_\text{i}}$ and $\varphi_{\text{S}_\text{e}}$). This measurement error is considered proportional to the flux value, and it is often assumed that two successive measurement errors are statistically independent. In the same manner as in the study [8], this uncertainty on the heat flux will be equal to $\sigma_\varphi = 3\%$ in the application section, and the statistical law of $\varepsilon_\varphi^{\text{mes}}$ can be written as follows:

$$\varepsilon_\varphi^{\text{mes}} \sim \mathcal{N}\left(\boldsymbol{0}, \sigma_\varphi^2 \begin{bmatrix} (y_1^{\text{mes}})^2 & 0 & \cdots & 0 \\ 0 & (y_2^{\text{mes}})^2 & \ddots & \vdots \\ \vdots & \ddots & \ddots & 0 \\ 0 & \cdots & 0 & (y_{\text{N}^{\max_\text{t}}}^{\text{mes}})^2 \end{bmatrix}\right). \tag{16}$$

where we recall that $\text{N}^{\max_\text{t}} = 2\text{N}_\text{t}$ if we have access to measurements of $\varphi_{\text{S}_\text{i}}$ and $\varphi_{\text{S}_\text{e}}$, and $\text{N}^{\max_\text{t}} = \text{N}_\text{t}$ when only the measurements of $\varphi_{\text{S}_\text{i}}$ are available.

3.2.2. Measurement error associated with the imposed temperatures

The second error term, $\varepsilon_T^{\text{mes}}$, is associated with the temperature error measurements on the interior and exterior surfaces. Indeed, in the proposed formalism, T_{S_i} and T_{S_e} are imposed to ensure the independence of the thermal equations to the heat transfer coefficients. However, these temperatures are not exactly known, but measured by sensors. According to the study [8], the uncertainty on this measured value of the temperature is close to σ_T=0.5 °C. These measurement errors can again be considered Gaussian, so if we denote $\boldsymbol{T}_{\text{S}_\text{i}}^{\text{mes}}$ and $\boldsymbol{T}_{\text{S}_\text{e}}^{\text{mes}}$ as the measured values of T_{S_i} and T_{S_e} at the N_t discretisation times, then we can write

$$\boldsymbol{T}_{\text{S}_\text{i}}^{\text{mes}} \sim \mathcal{N}\left(\begin{pmatrix} T_{\text{S}_\text{i}}(t_1) \\ \vdots \\ T_{\text{S}_\text{i}}(t_{\text{N}_\text{t}}) \end{pmatrix}, \sigma_T^2 \boldsymbol{I}_{\text{N}_\text{t}}\right), \quad \boldsymbol{T}_{\text{S}_\text{e}}^{\text{mes}} \sim \mathcal{N}\left(\begin{pmatrix} T_{\text{S}_\text{e}}(t_1) \\ \vdots \\ T_{\text{S}_\text{e}}(t_{\text{N}_\text{t}}) \end{pmatrix}, \sigma_T^2 \boldsymbol{I}_{\text{N}_\text{t}}\right), \tag{17}$$

where $\boldsymbol{I}_{\text{N}_\text{t}}$ is the $(N_t \times N_t)$-dimensional identity matrix. However, thermal dynamic simulation shows that the direct replacement of T_{S_i} and T_{S_e} by their noisy measured values in $\boldsymbol{u}^{\text{1D}}$ results in amplified noise on simulated heat flux values. In order to limit this phenomenon, we propose a two-stage approach: first, we smooth the measured values of T_{S_i} and T_{S_e}, using the information

on measurement noise (see Appendix C for the details of the proposed smoothing technique). The smoothing procedure under consideration then provides a mean value for the smoothed values of T_{S_i} and T_{S_e}, which are denoted by $T_{S_i}^{\text{Smooth}}$ and $T_{S_e}^{\text{Smooth}}$. But it can also provide independent evolution of T_{S_i} and T_{S_e} that are consistent with the available measurements of T_{S_i} and T_{S_e}, which can then be used to quantify the error committed by replacing T_{S_i} and T_{S_e} with $T_{S_i}^{\text{Smooth}}$ and $T_{S_e}^{\text{Smooth}}$, so that:

$$\boldsymbol{u}^{\text{1D}}(\boldsymbol{z}; T_{S_i}, T_{S_e}, T_w^{\text{Poly}}) = \boldsymbol{u}^{\text{1D}}(\boldsymbol{z}; T_{S_i}^{\text{Smooth}}, T_{S_e}^{\text{Smooth}}, T_w^{\text{Poly}}) + \varepsilon_T^{\text{mes}}, \tag{18}$$

$$\varepsilon_T^{\text{mes}} \sim \mathcal{N}\left(\mathbf{0}, \boldsymbol{\Sigma}_T\right), \quad \boldsymbol{\Sigma}_T = \frac{1}{Q}\sum_{q=1}^{Q} \boldsymbol{D}_{\varphi,q}\boldsymbol{D}_{\varphi,q}^T, \tag{19}$$

$$\boldsymbol{D}_{\varphi,q} = \boldsymbol{u}^{\text{1D}}(\boldsymbol{z}; T_{S_i}^{\text{Smooth}}, T_{S_e}^{\text{Smooth}}, T_w^{\text{Poly}}) - \boldsymbol{u}^{\text{1D}}(\boldsymbol{z}; T_{S_i,q}^{\text{Smooth}}, T_{S_e,q}^{\text{Smooth}}, T_w^{\text{Poly}}), \tag{20}$$

where $\left\{T_{S_i,q}^{\text{Smooth}}, T_{S_e,q}^{\text{Smooth}}\right\}_{q=1}^{Q}$ gathers Q likely evolutions of T_{S_i} and T_{S_e}, as explained in Appendix C.

3.2.3. Construction of the multi-fidelity meta-model and the uncertainty associated

As explained in Section 3.1, the estimation of $\boldsymbol{z}$ by a MH algorithm requires a very large number of calls to the thermal direct model. In order to obtain an estimate of $\pi(\boldsymbol{z}|\boldsymbol{y}^{\text{mes}})$ in a reasonable time, we proposed replacing $\boldsymbol{u}^{\text{1D}}$ with a meta-model. This replacement is responsible for the third error term $\varepsilon^{\text{Meta}}$ in Eq. (12). To construct this meta-model, we assume a Gaussian prior distribution for the vector-valued function $\boldsymbol{z} \mapsto \boldsymbol{u}^{\text{1D}}(\boldsymbol{z}; T_{S_i}^{\text{Smooth}}, T_{S_e}^{\text{Smooth}}, T_w^{\text{Poly}})$. This means that the vector $\boldsymbol{u}^{\text{1D}}(\boldsymbol{z}; T_{S_i}^{\text{Smooth}}, T_{S_e}^{\text{Smooth}}, T_w^{\text{Poly}})$ (discretised at the N_t measurement instants) is seen as a particular realisation of a Gaussian Process (GP) $\boldsymbol{Y}$ with values in $\mathbb{R}^{N_t^{\max}}$,

$$\boldsymbol{Y} \sim \text{GP}(\boldsymbol{\mu}, \boldsymbol{C}), \tag{21}$$

where $\boldsymbol{z} \mapsto \boldsymbol{\mu}(\boldsymbol{z})$ and $(\boldsymbol{z}, \boldsymbol{z}') \mapsto \boldsymbol{C}(\boldsymbol{z}, \boldsymbol{z}')$ are respectively the mean function and the covariance function of $\boldsymbol{Y}$. We then update this prior distribution by forcing $\boldsymbol{Y}$ to pass through M evaluations of the 1D thermal model in well-distributed values of $\boldsymbol{z}$ in Ω (see [47] for more details on how to build space-filling designs of experiments). Let

$$\mathcal{D}_M = \left\{(\boldsymbol{z}_m, \boldsymbol{u}^{\text{1D}}(\boldsymbol{z}_m; T_{S_i}^{\text{Smooth}}, T_{S_e}^{\text{Smooth}}, T_w^{\text{Poly}})),\ 1 \le m \le M\right\}$$

be the set gathering these M code evaluations. For these different evaluations, it is important to note that only the values of $\boldsymbol{z}$ change (the values of $T_{S_i}^{\text{Smooth}}, T_{S_e}^{\text{Smooth}}, T_w^{\text{Poly}}$ remain the same). The conditional GP is thus defined by

$$\boldsymbol{Y} \mid \mathcal{D}_M \sim \text{GP}\left(\boldsymbol{\mu}_c, \boldsymbol{C}_c\right), \tag{22}$$

where the expressions of the posterior mean function, $\boldsymbol{\mu}_c$, and of the posterior covariance function, $\boldsymbol{C}_c$ can explicitly be derived (see [48,49] for more details). Noting $\boldsymbol{u}^{\text{meta}}(\boldsymbol{z}) = \boldsymbol{\mu}_c(\boldsymbol{z})$ the constructed meta-model and $\boldsymbol{\Sigma}_{\text{meta}}(\boldsymbol{z}) = \boldsymbol{C}_c(\boldsymbol{z}, \boldsymbol{z})$, we recover the notations involved in the Bayesian formalism expressions of Section 3.1.

The relevance of a multi-fidelity meta-model strongly depends on the choice of $\boldsymbol{\mu}$ and $\boldsymbol{C}$. In this work, we first choose for the mean function

$$\boldsymbol{\mu}(\boldsymbol{z}) = \alpha \times \boldsymbol{u}^{\text{RC}}(\boldsymbol{z}; T_{S_i}^{\text{Smooth}}, T_{S_e}^{\text{Smooth}}, T_w^{\text{Poly}}), \tag{23}$$

where α is a parameter to be adjusted corresponding to the coefficient of correlation between the high fidelity model (1D model) and the low fidelity model (RC model), and $\boldsymbol{u}^{\text{RC}}$ corresponds to the discretisation of the output of the RC model with 5 resistances and 4 capacitance presented in Fig. 3 (see Appendix D for the detailed description of the RC model and the relation between the different characteristics of the RC model, the input vector $\boldsymbol{z}$ and the output vector $\boldsymbol{u}^{\text{RC}}$). The use of RC models is standard practice in the world of building engineering. We thus obtain simplified models that are very fast to calculate and which clearly reflect the main physical phenomena involved. By adding the estimated α, we give ourselves the possibility of making the meta-model more or less based on this RC model: if the RC model turns out to be very close to the 1D model, then we can take a value of α close to 1, and if this is ultimately not the case, the value of α can be chosen close to 0.

Concerning the choice of the covariance matrix, as explained in [50,51], it can be very practical to separate the dependence in time and in $\boldsymbol{z}$ in the modelling of the function $\boldsymbol{C}$, so that for all $\boldsymbol{z}, \boldsymbol{z}' \in \Omega$,

$$\boldsymbol{C}(\boldsymbol{z}, \boldsymbol{z}') = \boldsymbol{R}_t \times C_z(\boldsymbol{z}, \boldsymbol{z}'), \tag{24}$$

where $\boldsymbol{R}_t$ is a $(N_t^{\max} \times N_t^{\max})$-dimensional positive definite matrix, and C_z is any real-valued covariance function. In this work, we will limit ourselves to the Matérn-5/2 class of covariance functions (see [49] for alternative choices),

$$C_z(\boldsymbol{z}, \boldsymbol{z}') = \left(1 + \sqrt{5}h(\boldsymbol{z}, \boldsymbol{z}') + \frac{5}{3}h(\boldsymbol{z}, \boldsymbol{z}')^2\right)\exp\left(-\sqrt{5}h(\boldsymbol{z}, \boldsymbol{z}')\right), \tag{25}$$

$$h(\boldsymbol{z}, \boldsymbol{z}') := \|\text{diag}(\boldsymbol{\ell})^{-1}(\boldsymbol{z} - \boldsymbol{z}')\|, \quad \text{diag}(\boldsymbol{\ell}) = \begin{bmatrix} \ell_1 & 0 & \cdots & 0 \\ 0 & \ell_2 & \ddots & \vdots \\ \vdots & \ddots & \ddots & 0 \\ 0 & \cdots & 0 & \ell_{d_z} \end{bmatrix}, \tag{26}$$

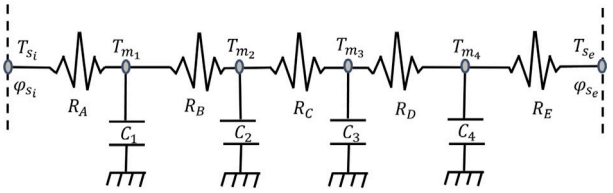

Fig. 3. Low fidelity model corresponding to a model with 5 resistances and 4 capacitance (R5C4).

where $\|.\|$ is the classical Euclidean norm, and the vector $\boldsymbol{\ell} = (\ell_1, \ldots, \ell_{d_z})$ is a d_z-dimensional vector that also needs to be adjusted to the data with $\ell_{d_z} = 8$ corresponding to the number of parameters to identify. The construction of the meta-model is ultimately based on the estimation of α, $\boldsymbol{R}_t$ and $\boldsymbol{\ell}$ from the M evaluations of the 1D code. In this work, all these quantities are estimated by maximising the likelihood, as explained in detail in [51]. To limit the problems of generalisation, it is important to notice that the meta-model is created as a function of the measured and imposed boundary condition temperatures and the initial temperature of the wall (see Section 3.1). This means that a meta-model needs to be created (with associated values of the hyperparameters α, $\boldsymbol{R}_t$ and $\boldsymbol{\ell}$) for each test performed, *i.e.* for each wall and each specific weather conditions. The fact that the hyperparameters of this meta-model may not be perfectly well estimated will also be taken into account by adding a model error term, which will be described in the next section.

3.2.4. Model error

The fourth and final error term ε^{Res} in Eq. (12) is called residual error, in the sense that it models the difference that may remain between $\boldsymbol{y}$ and $\boldsymbol{u}^{\text{Meta}}(\boldsymbol{z}; T_{\text{S}_\text{i}}^{\text{Smooth}}, T_{\text{S}_\text{e}}^{\text{Smooth}}, T_{\text{w}}^{\text{Poly}})$ once the three previous errors have been removed. Characterising this error is not easy, because it symbolises everything that we do not know or do not control. In this work, we then propose to decompose this model error into two Gaussian terms for each measured output $\varphi_{\text{S}_\text{i}}$ and $\varphi_{\text{S}_\text{e}}$: two classic additive errors of variance $\theta_{\text{a,i}}^2$ and $\theta_{\text{a,e}}^2$, plus two multiplicative errors of variance $\theta_{\text{m,i}}^2$ and $\theta_{\text{m,e}}^2$. In the case when we have access to the measurements of $\varphi_{\text{S}_\text{i}}$ and $\varphi_{\text{S}_\text{e}}$ (i.e. $N_t^{max} = 2N_t$), we then write $\boldsymbol{\varepsilon}^{\text{Res}} = (\boldsymbol{\varepsilon}_{\varphi_{S_i}}^{\text{Res}}, \boldsymbol{\varepsilon}_{\varphi_{S_e}}^{\text{Res}})$,

$$\boldsymbol{\varepsilon}_{\varphi_{S_i}}^{\text{Res}} \sim \mathcal{N}\left(\mathbf{0}, \theta_{\text{a,i}}^2 \boldsymbol{I}_{\text{N}_\text{t}} + \theta_{\text{m,i}}^2 \begin{bmatrix} (y_1^{\text{mes}})^2 & 0 & \cdots & 0 \\ 0 & (y_2^{\text{mes}})^2 & \ddots & \vdots \\ \vdots & \ddots & \ddots & 0 \\ 0 & \cdots & 0 & (y_{\text{N}_\text{t}}^{\text{mes}})^2 \end{bmatrix}\right), \tag{27}$$

$$\boldsymbol{\varepsilon}_{\varphi_{S_e}}^{\text{Res}} \sim \mathcal{N}\left(\mathbf{0}, \theta_{\text{a,e}}^2 \boldsymbol{I}_{\text{N}_\text{t}} + \theta_{\text{m,e}}^2 \begin{bmatrix} (y_1^{\text{mes}} + N_t)^2 & 0 & \cdots & 0 \\ 0 & (y_2^{\text{mes}} + N_t)^2 & \ddots & \vdots \\ \vdots & \ddots & \ddots & 0 \\ 0 & \cdots & 0 & (y_{2\text{N}_\text{t}}^{\text{mes}})^2 \end{bmatrix}\right). \tag{28}$$

Four new parameters ($\theta_{\text{a,i}}$, $\theta_{\text{a,e}}$, $\theta_{\text{m,i}}$ and $\theta_{\text{m,e}}$) are thus introduced to model the link between measurements and outputs of the meta-model. The matrix $\boldsymbol{W}(\boldsymbol{z})$ introduced in Eq. (13) now depends on these four parameters, and consequently the likelihood function $\pi(\boldsymbol{y}^{\text{mes}}|\boldsymbol{z})$ also depends on them. Once the matrix $\boldsymbol{\Sigma}_\varphi$ has been constructed, once the smoothing of T_{S_i} and T_{S_e} have been carried out and the error propagated for the construction of $\boldsymbol{\Sigma}_T$, and once the parameters $(\alpha, \boldsymbol{R}_t, \boldsymbol{\ell})$ of the meta-model have been estimated from M dedicated evaluations of the 1D model, we finally propose, once again, to estimate $\theta_{\text{a,i}}$, $\theta_{\text{a,e}}$, $\theta_{\text{m,i}}$ and $\theta_{\text{m,e}}$ by their likelihood maximisation estimators $\theta_{\text{a,i}}^{\text{MLE}}$, $\theta_{\text{a,e}}^{\text{MLE}}$, $\theta_{\text{m,i}}^{\text{MLE}}$ and $\theta_{\text{m,e}}^{\text{MLE}}$, so that

$$(\theta_{\text{a,i}}^{\text{MLE}}, \theta_{\text{a,e}}^{\text{MLE}}, \theta_{\text{m,i}}^{\text{MLE}}, \theta_{\text{m,e}}^{\text{MLE}}, \boldsymbol{z}^{\text{MLE}}) \in \arg \max_{(\theta_1, \theta_2, \boldsymbol{z}) \in (0,\infty)\times(0,\infty)\times\mathbb{R}^+} \pi(\boldsymbol{y}^{\text{mes}}|\boldsymbol{z}). \tag{29}$$

By fixing the four parameters that characterise the model error to their maximum likelihood estimators, we neglect the uncertainty associated with their estimation. This strongly accelerates the convergence of the MCMC algorithm that is used to infer the posterior distribution of the thermal properties, but this may be done at the price of a little over or under estimation of the obtained credible intervals.

3.2.5. Summary of the proposed Bayesian method

The Bayesian approach proposed for estimating the thermal properties of an IIW involves several models and approximations, which we propose to summarise in this section. In accordance with Fig. 4, this approach can be decomposed into several steps.

- Step 1 : A stabilisation phase (before excitation) is first considered from t_0^S to t_0 to reduce the influence of the unknown initial temperature in the considered wall. The excitation phase at the interior surface then starts at t_0 and ends at t_f. We extract from these two phases the inside and outside measurements of the surface temperatures and thermal fluxes. From the measurements at t_0^S, the temperature in the wall is approximated by a piece-wise polynomial function T_w^{Poly}.

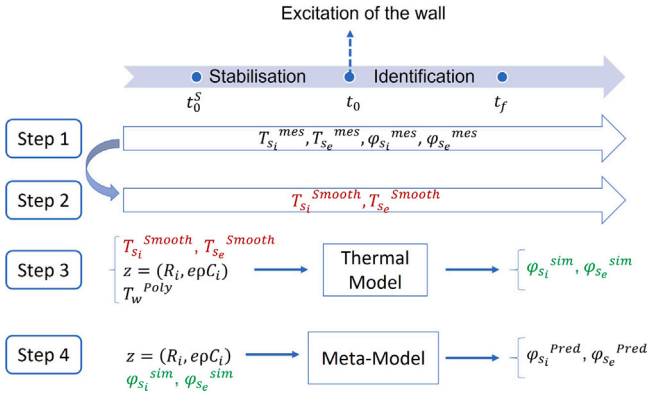

Fig. 4. General scheme for processing simulated and measured data to identify the thermal properties of the wall.

Table 1
Ranges of possible values for IIW for the parameters of the 1D model corresponding to : the thickness (e_i in m), the thermal resistance (R_i in m^2 K/W) and the thermal capacitance ($e\rho C_i$ in kJ/Km^2).

Layer - #*i*	e_i	R_i	$e\rho C_i$
#1 Internal coating	$0.01 \leq e_1 \leq 0.03$	$0.0125 \leq R_1 \leq 0.15$	$6 \leq e\rho C_1 \leq 45$
#2 Insulation	$0.04 \leq e_2 \leq 0.2$	$0.66 \leq R_2 \leq 10$	$1.08 \leq e\rho C_2 \leq 42$
#3 Support wall	$0.15 \leq e_3 \leq 0.3$	$0.065 \leq R_3 \leq 3$	$97.5 \leq e\rho C_3 \leq 750$
#4 External coating	$0.01 \leq e_4 \leq 0.03$	$0.0055 \leq R_4 \leq 0.3$	$5 \leq e\rho C_4 \leq 60$

- Step 2 : These measurements are noisy. For this reason, we propose to smooth the measured temperatures of the inner surface ($T_{S_i}^{Smooth}$) and the outer surface ($T_{S_e}^{Smooth}$) before using them in the thermal direct model. The uncertainties coming from this smoothing are also quantified at this step.
- Step 3 : The 1D thermal problem is then rewritten to take the smoothed surface temperatures as boundary conditions, and the temperature field T_w^{Poly} as initial condition. In order to be executed, this direct model requires the definition of the vector $\boldsymbol{z}$ that gathers the quantities to be estimated, and returns the heat fluxes on the interior and exterior wall faces.
- Step 4 : Finally, we construct the multi-fidelity meta-model from M calls to the RC and 1D models. It is this meta-model which will finally be used to make the link between measurements and predictions based on $\boldsymbol{z}$.

4. Applications

Numerical and experimental applications of the method proposed in Section 3 are presented. In Section 4.1, a few representative walls in different weather conditions and different configurations are numerically studied. The ranges of possible values for the physical properties of IIW to be identified are provided by the study [7] and presented in Table 1. These ranges have been established for building materials commonly used in these types of wall components. Lastly in order to validate the proposed identification method, an application on experimental data is presented in Section 4.2.

To identify the wall thermal resistance in a reasonable time (less than 24 h) using the Bayesian inverse modelling technique presented in Section 3, we consider: (i) a controlled excitation of 400 W/m^2 over a diameter of 60 cm on the inner wall surface, (ii) a data acquisition rate of 2 min and (iii) common computational resources, *e.g.* a laptop. In general, the estimation results will be reported in tables gathering the most likely estimate and credible intervals at the 95% level in square brackets. We insist on the fact that these credible intervals are themselves approximations, as they simply correspond to the 2.5% and 97.5% empirical quantiles estimated on all the values returned by the MCMC algorithm. As such, they indicate a zone with a high probability (here around 95%) of containing the true value to be estimated.

4.1. Study on simulated wall data

4.1.1. Presentation of the studied configurations

The method is numerically tested for two winter weather conditions:

- M_1 denotes a typical southern French climate in Carpentras over a 6-day period from September 28th to October 4th, which is taken from the 2012 French thermal regulations [5]. A south-facing orientation is considered;
- M_2 denotes a typical northeastern French climate in Nancy over a 6-day period from November 28th to December 4th taken from the 2012 French thermal regulations [5]. A north-facing orientation is considered.

Table 2
Thermal properties of the walls studied (e_i in m, R_i in m^2 K/W and $e\rho C_i$ in kJ/(K m^2)).

Walls	e_1	e_2	e_3	e_4	R_1	R_2	R_3	R_4	$e\rho C_1$	$e\rho C_2$	$e\rho C_3$	$e\rho C_4$
W_1	0.01	0.04	0.15	0.01	0.01	0.83	0.06	0.01	10	2	360	9
W_2	0.01	0.14	0.20	0.01	0.05	4.37	0.28	0.02	9.7	5.7	160	15
W_3	0.01	0.20	0.22	0.02	0.05	8.00	0.55	0.02	9.7	6	220	18
W_4	0.03	0.20	0.30	0.03	0.04	3.33	0.13	0.02	45	42	750	60

Table 3
Configurations tested using different stabilisation times (in h), excitation times (in h) and available measurements.

Configuration	Stabilisation time (h)	Excitation time (h)	Available measurements
$\boldsymbol{C_1}$	**72**	**72**	$\boldsymbol{\varphi_{S_i}, \varphi_{S_e}}$
C_2	72	72	φ_{S_i}
C_3	0	72	$\varphi_{S_i}, \varphi_{S_e}$
C_4	0	72	φ_{S_i}
C_5	0	10	$\varphi_{S_i}, \varphi_{S_e}$
C_6	0	10	φ_{S_i}

In Fig. 5, the time evolution of the outdoor temperatures T_{ext} and solar fluxes Φ_{sun} for the 3 last days (excitation phase) are presented for the two weather conditions (Nancy and Carpentras). As expected, T_{ext} and Φ_{sun} are significantly higher in the case of Carpentras throughout the entire study period.

The proposed method is applied to estimate the thermal properties of four reference internal insulated walls (IIW) with given thermal properties and total thickness ($e_{Tot} = e_1 + e_2 + e_3 + e_4$) and submitted to the two considered weather conditions. These walls are noted W_j, with $j \in [\![1;4]\!]$, and are chosen so that

1. W_1 is poorly insulated ($R_{Tot} = 0.91$ m^2 K/W) and has a low total thickness ($e_{Tot} = 0.21$ m),
2. W_2 has a better insulation ($R_{Tot} = 4.72$ m^2 K/W) and a common total thickness ($e_{Tot} = 0.36$ m),
3. W_3 is highly insulated ($R_{Tot} = 8.62$ m^2 K/W) while having a large total thickness ($e_{Tot} = 0.45$ m),
4. W_4 is of medium insulation ($R_{Tot} = 3.51$ m^2 K/W) and has a large total thickness ($e_{Tot} = 0.56$ m).

Here, the measurements are simulated using a 3D thermal model, and noise is added to the measured outputs T_{S_i}, T_{S_e}, φ_{S_i} and φ_{S_e}. The measurement error is of the order of 0.5 W/m^2 for φ_{S_i} (respectively 1.4 W/m^2 for φ_{S_e}) in the case of Carpentras and of the order of 0.5 W/m^2 for φ_{S_i} (respectively 0.3 W/m^2 for φ_{S_e}) in the case of Nancy. The measurement error of the temperatures (T_{S_i}, T_{S_e}) is close to 0.5 °C (see Section 3.2.2). The reference values of the eight parameters characterising the thermal properties of these four reference walls are presented in Table 2.

According to Sections 2.2 and 2.3, the measured surface temperatures (T_{S_i} and T_{S_e}) are imposed as boundary conditions in the wall thermal models to achieve independence from the exchange coefficients in the inversion process. However, since the measurements are noisy, imposing them directly in the 1D and RC simulations results in significant fluctuations in the surface thermal fluxes (φ_{S_i} and φ_{S_e}). To avoid such a pathological phenomenon and as explained in Section 3.2.2, a smoothing is applied to the measurements before imposing them as boundary conditions (for more details see Appendix E).

A comparison of the thermal responses of the 3D (considered as the measurement in the following), 1D and RC models for the same wall properties is shown in Fig. 6. We note that the difference between the 3D (in black) and 1D (in red) models is relatively small in the case of W_2. Moreover, we observe a strong correlation between the 1D and RC models in the cases of φ_{S_i} and φ_{S_e}, which justifies the choice of constructing the predictor of the 1D model as a linear combination of the RC model plus a discrepancy term modelled by a centred Gaussian process (see Section 3.2.3).

To investigate the robustness of the proposed method to

- the stabilisation phase,
- the initial temperature in the wall,
- the duration of the excitation,
- and the fact that only partial instrumentation are available,

we now consider six different configurations, whose characteristics are presented in Table 3. We note $M_k C_\ell W_j$ the numerical test associated with the wall W_j with $j \in [\![1;4]\!]$ (see Table 2), the weather "k" ($k = 1$ for Carpentras and $k = 2$ for Nancy), and the configuration "ℓ" ($\ell \in [\![1;6]\!]$). For example, the test $M_1 C_1 W_2$ corresponds to wall W_2, for Carpentras weather, when considering the first configuration, that is to say a stabilisation time of 72 h, an excitation time of 72 h, and ($\varphi_{S_i}, \varphi_{S_e}$) as available measurements.

For each wall tested, a meta-model is created (see Section 4.1.2) based on the multi-fidelity approach described in Section 3.2.3. It should be noted that the model generating the measurements (3D thermal model) is not the same as those used for the inversion (1D and RC models), which justifies the inclusion of the corrective modelling error term ε^{Res} presented in Section 3.2. Based on the created meta-model, the method described in Section 3.1 is used for estimating the total thermal resistance (R_{Tot}) and quantifying its precision (see Section 4.1.5).

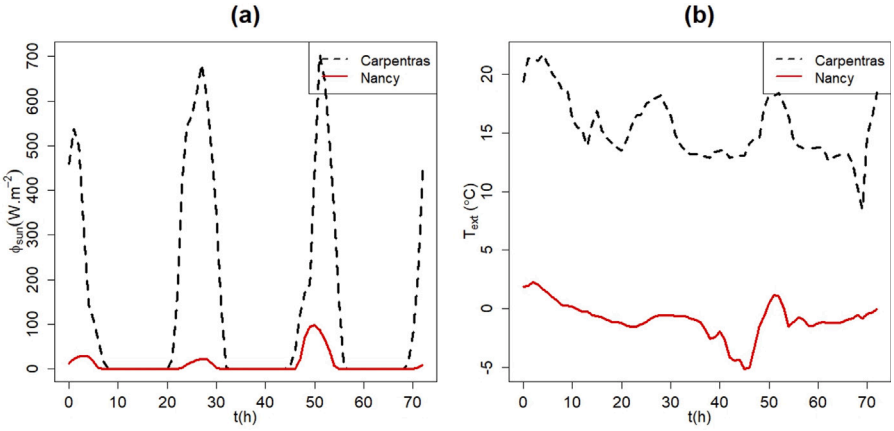

Fig. 5. Weather data (Nancy and Carpentras) over time (3 last days): (a) Solar flux, (b) Outdoor temperature.

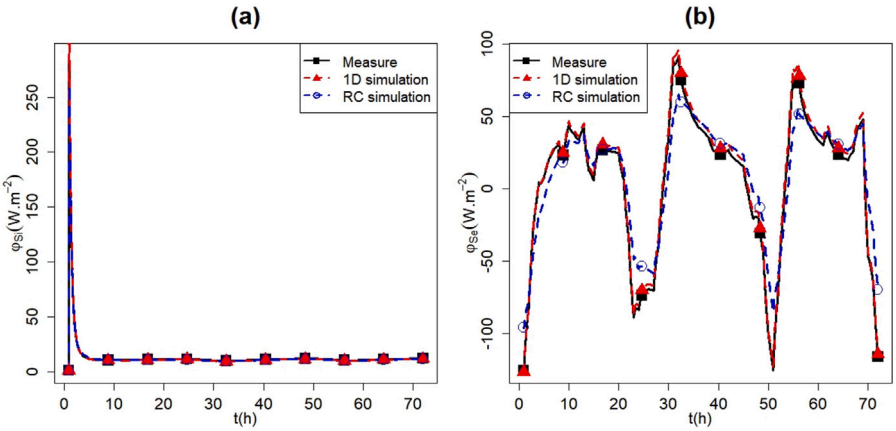

Fig. 6. Comparison of generated outputs with different models in the case of Carpentras, wall 2: (a) φ_{S_i}, (b) φ_{S_e}.

Table 4
Study of the prediction quality of φ_{S_i} and φ_{S_e} based on the indicators: RMSE, MAE, for the four walls studied in weather M_1 and configuration C_1.

Indicator	$M_1C_1W_1$		$M_1C_1W_2$		$M_1C_1W_3$		$M_1C_1W_4$	
	φ_{S_i}	φ_{S_e}	φ_{S_i}	φ_{S_e}	φ_{S_i}	φ_{S_e}	φ_{S_i}	φ_{S_e}
RMSE	0.10	0.13	0.14	0.24	0.13	0.25	0.09	0.18
MAE	0.05	0.06	0.06	0.12	0.06	0.12	0.03	0.08

4.1.2. Construction of the meta-model

Meta-models are proposed to fastly compute the quantities of interest φ_{S_i} and φ_{S_e} that are used in the estimation of total resistance.

Based on conventional sensitivity analyses, such as Sobol-type variance decomposition analyses [52], it turns out that certain model parameters of the vector $\boldsymbol{z}$ to be estimated have a low influence on internal and external heat fluxes. Therefore, these model parameters can be fixed at nominal values to simplify the construction of the meta-model.

More precisely, the φ_{S_i} predictor is created using only 5 of the 8 components of $\boldsymbol{z}$: the parameters of layers 1 and 2 (R_1, R_2, $e\rho C_1$ and $e\rho C_2$) and the resistance of the third layer (R_3). And the predictor of φ_{S_e} is also created using only 5 components of $\boldsymbol{z}$, but not the same: the resistance of the second layer (R_2), and the parameters of the third and fourth layers (R_3, R_4, $e\rho C_3$ and $e\rho C_4$).

The performance indicators RMSE*, the root mean square of the average over time of the error, and MAE*, the mean absolute value of the average over time of the error have been calculated to quantify the quality of the constructed meta-models. Note that the meta-models are built using 4000 1D and RC thermal dynamic simulations, then tested on a different test set of size $n = 1000$.

Table 4 shows the values of the performance indicators for the prediction of φ_{S_i} and φ_{S_e} in the first configuration C_1 for the weather condition M_1 and for each wall tested (similar results were obtained for the other tested configuration and weather

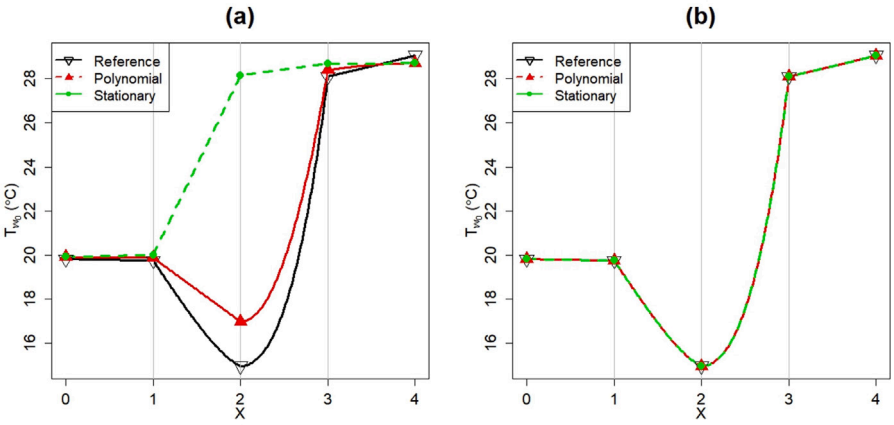

Fig. 7. Comparison of initial wall temperatures (presented in the normalised coordinate $X \in [0,4]$ in the wall) calculated with a 3-days unsteady calculation (taken as reference), polynomial and stationary in both cases: without (a) and with (b) a stabilisation phase in the case of W_2, weather Carpentras M1.

condition). Let us recall that the configurations, the weather conditions and the studied walls are defined in Section 4.1.1. We note a very accurate prediction quality for the wide variety of walls tested with thicknesses varying from 0.21 m to 0.56 m and with thermal resistances from 0.91 m^2 K/W to 8.62 m^2 K/W. In addition, we see that the uncertainty associated with the meta-model is smaller than the measurement error (see Section 4.1.6). It allows the computation time of the 1D direct model ($\approx$ 21 seconds per simulation using a standard computer with Intel(R) Core (TM) i7-1185G7 @ 3.00 GHz) to be divided by more than 50.

4.1.3. Influence of the temperature initial conditions and the stabilisation phase

As explained in Section 2.4, the initial temperature in the wall is unknown, and it is expected that incorrect initialisation of the wall temperature in the thermal calculations could alter the estimates of the thermal properties of the walls studied. Consequently, we propose to use a stabilisation period of 3 days before starting the active sollicitation on the internal wall surface. As in operational purposes the 3-day stabilisation period may be not possible, we also propose an enhanced approximate of the temperature profile in the initial state by a piecewise polynomial function (see Section 2.4 and Appendix A). To illustrate the benefits of the polynomial initialisation and the proposed stabilisation phase, Fig. 7 compares the wall temperatures obtained : (i) when the model is initialised with the "true" wall temperature (in black, which serves as a reference) obtained by an unsteady computation, (ii) when the model is initialised with the commonly used assumption of stationarity of the flux in the wall (in green), or (iii) when the proposed polynomial profile is used (in red), both with and without stabilisation in the case of Carpentras and for the wall W_2. We first note in this figure that using polynomial profiles leads to temperatures in the wall that are relatively close to the reference. This is not the case when using an initial temperature from a steady-state calculation. Nevertheless, we see in Fig. 7-(b) that these differences almost disappear when considering the stabilisation phase of 3 days. This last conclusion is in agreement with the work achieved in [39], which also showed that a 3-day stabilisation was able to cancel the influence of the initial wall temperature on the identification results.

4.1.4. Identification results for wall 2

In this section we apply the proposed method to the $M_1C_1W_2$ test. The wall W2 was chosen because it corresponds to a standard wall of average thickness and resistance (see Table 2). We first consider the recommended configuration test C_1 (3 days of stabilisation + 3 days of excitation, using measurements of φ_{S_i} and φ_{S_e}) in the case of Carpentras weather, which is a climate with more outdoor temperature and solar irradiance variations. All the other tests are presented in Section 4.1.5. The identification of the 8 parameters (the thermal resistances and capacitance of each layer) is presented in Table 5 and Fig. 8. It can be seen that the resistances of the first two layers (R_1, R_2) are estimated with great accuracy (small uncertainty), which is very satisfying as the insulation resistance R_2 is the parameter of most interest. On the other hand, the resistances of layers 3 and 4 (R_3, R_4) are estimated with more uncertainty (but still acceptable, i.e. the gap between the reference and the estimated values is less than 0.2 m^2 K/W). The identification of the total thermal resistance of W_2 (which is the objective of this study) is very relevant with low uncertainties. For thermal comfort purposes, we also notice that the total heat capacity ($e\rho C_{\mathrm{Tot}}$) of W_2 is estimated in a satisfactory manner, with an acceptable credible interval. This means that for this particular case $M_1C_1W_2$, the proposed method is able to estimate not only R_{Tot}, but also to provide a good estimation of the wall thermal capacitance.

As a complement, Fig. 9 shows correlations between pairs of model parameters, which can highlight potential compensation phenomena during the estimation phase. For instance, we first see that there is a negative correlation between the thermal resistances, especially R_2 and R_3, which can increase the uncertainty of parameter estimates. The thermal resistances and the thermal capacitance of the third (R_3, $e\rho C_3$) and fourth (R_4, $e\rho C_4$) layers are strongly positively correlated. This suggests that the uncertainties in the estimates of R_3 and R_4 may be responsible for the large uncertainties in the estimates of $e\rho C_3$ and $e\rho C_4$. From a thermal comfort point of view, the thermal capacitance of the support wall is the most important to determine (as it is the major contributor). For this reason, a large uncertainty in the estimate of $e\rho C_3$ is the main source of a large credible interval for the estimate of $e\rho C_{\mathrm{Tot}}$.

Table 5
Identification of the thermal resistance (in m^2 $K.W^{-1}$) and the thermal capacitance (in kJ K^{-1} m^{-2}) of each layer in the case of test $M_1C_1W_2$. The values in square brackets define the 95% credible intervals, while the estimated values correspond to the values maximising the *a posteriori* PDF, i.e. the most likely values given the available measurements.

Layer	R^{Ref}	R^{Est}	$e\rho C^{Ref}$	$e\rho C^{Est}$
#1 - Internal coating	0.05	0.06[0.05; 0.07]	9.7	9.22[8.82; 9.64]
#2 - Insulation	**4.37**	**4.20[4.05; 4.36]**	5.7	4.98[3.67; 7.18]
#3 - Wall support	0.28	0.24[0.16; 0.32]	**160**	**120[100; 166]**
#4 - External coating	0.008	0.04[0.01; 0.07]	15	39.1[15.5; 57.3]
Total Wall	**4.72**	**4.53[4.41; 4.70]**	**190**	**171[151; 211]**

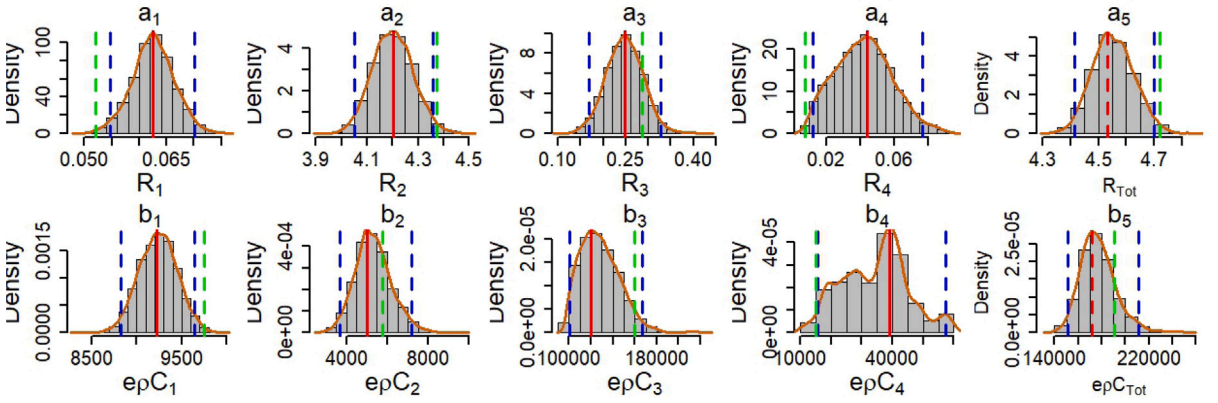

Fig. 8. Identification results in the case $M_1C_1W_2$ for the thermal resistance (R_i in m^2 K/W) and the thermal capacity ($e\rho C_i$ in m J/(K m^3)). These results are presented in the form of histograms of a representative set of 5000 likely values of the parameters to be estimated using an MCMC approach. The graphs a_1 and b_1 are associated with the internal coating; a_2 and b_2 correspond to the insulation, a_3 and b_3 refer to the support wall, a_4 and b_4 characterise the external coating, and a_5 and b_5 correspond to the total wall. The approximation of the *a posteriori* distribution is shown in brown solid line, the red vertical line corresponds to the value that maximises the likelihood, the green vertical line is the reference value, while the blue vertical lines show the credible intervals with level 95%. (For interpretation of the references to colour in this figure legend, the reader is referred to the web version of this article.)

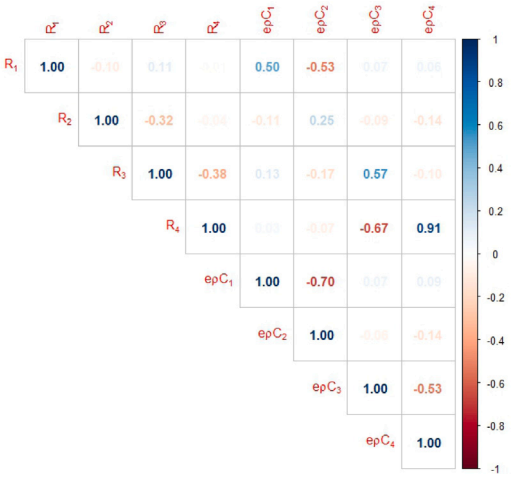

Fig. 9. Correlation matrix for the estimated parameters in the case of test $M_1C_1W_2$. The closer these values are to 1, the more positively correlated two quantities are, and conversely, the closer these values are to −1, the more negatively correlated two quantities are.

4.1.5. Study of different weather conditions and configurations

In this section, we aim to demonstrate the robustness of the proposed method for estimating the thermal properties of a variety of walls, potentially subject to very different conditions. Hence, we present estimation results for the 4 walls previously introduced, in the 6 considered configurations, and for the 2 weather conditions.

Application in the configuration C_1 for different weather conditions on walls with different thermal properties. To begin, Table 6 shows the estimated values of R_{Tot} and $e\rho C_{Tot}$ in the configuration C_1 for the weather conditions M_1 and M_2. Remember that C_1 is the configuration we particularly recommend, as it is based on the maximum number of observations (φ_{S_i} and φ_{S_e}) on a

Table 6
Identification of the total thermal resistances (R_{Tot} in m^2 K/W) and the total thermal capacitance ($e\rho C_{Tot}$ in kJ/(K m^2)) of the walls studied, in the configuration C_1 for the two weather conditions considered. The results are presented in the form MAP[IC$_{95\%}$] where MAP is the value which maximises the *a posteriori* distribution and [IC$_{95\%}$] is the credible interval at 95%.

Wall	W_1	W_2	W_3	W_4
R^{Ref}	0.91	4.72	8.62	3.51
$e\rho C^{Ref}$	380	190	250	890
M_1				
R^{Est}	1.13[1.08; 1.20]	4.53[4.41; 4.70]	8.00[7.26; 8.93]	2.97[2.73; 3.31]
$e\rho C^{Est}$	361[348; 373]	171[151; 211]	766[430; 791]	860[807; 891]
M_2				
R^{Est}	0.80[0.77; 0.82]	4.82[4.34; 5.08]	8.25[8.02; 8.52]	3.18[2.63; 4.05]
$e\rho C^{Est}$	353[151; 464]	195[158; 796]	762[632; 813]	647[464; 844]

large time interval and a sufficiently long stabilisation phase. The results provided by this table are quite satisfactory for poorly to highly internal insulated walls. The total thermal resistance R_{Tot} is estimated with a high accuracy for walls with total thicknesses varying between 0.21 m and 0.56 m and total thermal resistances varying between 0.91 m^2 K/W and 8.62 m^2 K/W regardless of the considered weather conditions (M_1 or M_2).

In parallel, the estimated values of $e\rho C_{Tot}$ for the walls W_1, W_2 and W_4 are rather close to the reference values. The results are note precise for W_3 walls, resulting in very large credible intervals. As already explained in the case of W_2 (see Section 4.1.4), the main source of these large uncertainties in the estimate of $e\rho C_{Tot}$ comes from the difficulty of the proposed approach (which consists in heating the wall from the inside surface) to precisely estimate the parameters associated with the third layer (support wall), that is behind the insulation layer. In fact, the identification of $e\rho C_3$ is particularly difficult for the wall W_3 which has a very high level of insulation ($R_2 = 8$ m^2 K/W). In conclusion, the approach proposed in this study makes it possible not only to identify the total thermal resistance of walls with different thermal properties when submitted to different weather conditions, but can also provide interesting information on the thermal capacitance of the wall with $R_{Tot} < 5$ m^2 K/W even if this was not the original aim.

Application in different configurations. The effectiveness of the proposed method in the configuration C_1 has been demonstrated for walls with different thermal properties and under different weather conditions M_1 and M_2. The aim of this section is now to quantify the relevance of the proposed method when used in more or less deteriorated conditions (reduced measurement time and fewer instruments used). To this end, Table 7 shows the results of the estimation of R_{Tot} and $e\rho C_{Tot}$ for the wall W_2 when considering the configurations listed in Table 3. First of all, we note that the use of a polynomial initial wall temperature, without taking into account a stabilisation phase (configurations C_3 and C_4), allows to obtain results for R_{Tot} close to the ones obtained with a stabilisation phase of 3 days (configurations C_1 and C_2), with slightly higher uncertainties. In other words, the use of a polynomial IC is a way to reduce the measurement time (from 6 days of measurements to 3 days without the stabilisation phase) without too much impact on the results. Furthermore, if the excitation time is long enough (in particular to ensure that the heating phase from the inside reaches the outside layers so that measurements are affected by the thermal properties of the outer layers), we obtain interesting estimations of R_{Tot} when only φ_{S_i} is recorded (configurations C_2, C_4 to be compared to configurations C_1, C_3). Thus, due to the instrumentation chosen (namely an imposed excitation of 400 W m^{-2} on the internal surface), we verify once again that it is indeed φ_{S_i}, more than φ_{S_e}, that largely enables the estimation of R_{Tot} in the case of an IIW. Finally, the further we deviate from the recommended configuration C_1, by reducing instrumentation or shortening measurement time, the greater the uncertainties on the estimated value of R_{Tot}. In the configuration where we have the least data (C_6), we are able to obtain information about the minimum resistance of the wall. Nevertheless, it should be noted that the true value of R_{Tot} is always close to the 95% credible intervals, hence it shows the interest of the proposed Bayesian approach for the different configurations tested (in particular to specify lower bounds on the total thermal resistance).

The conclusions drawn here in the case of W_2 are similar to those for the other walls tested, with slight exceptions in the case of the thickest wall W_4 where, in certain configurations, R^{Ref} is not within the credible interval obtained, but very close to its limits. The analysis of uncertainty quantification presented in the next section will provide physical explanations on the larger credible interval obtained for the wall W_4.

4.1.6. Uncertainty quantification

The Sections 4.1.4 and 4.1.5 present the identifications of R_{Tot} and $e\rho C_{Tot}$ as well as the credible intervals of the estimated parameters corresponding to the uncertainties considered. As already mentioned, one of the specific features of this study is that an uncertainty quantification is carried out to take into account the different sources of error that may affect the identification results. To this end, in this section we will compare the quantified uncertainties for different walls. Fig. 10 shows the evolution of the variance of the different considered errors as a function of time in the case of $M_1C_2W_2$ (a) and $M_1C_2W_4$ (b). In both cases (W_2 and W_4) the variance error associated with the propagation of the uncertainty of the measured temperatures (T_{S_i} and T_{S_e}) on the fluxes (ε_T^{mes}) is the smallest (even negligible), which implies that the applied smoothing is particularly effective in obtaining a very good

Table 7
Identification of the total thermal resistances (R_{Tot} in m² K/W) and the total thermal capacity ($e\rho C_{Tot}$ in kJ/(K m²)) of W_2, in the different configurations tested for the two weather conditions M_1 and M_2. The results are presented in the form MAP[$IC_{95\%}$] where MAP is the value which maximises the *a posteriori* distribution and [$IC_{95\%}$] is the credible interval at 95%.

Estimated parameters	R^{Est} (R^{Ref} = 4.72 m² K/W)		$e\rho C^{Est}$ ($e\rho C^{Ref}$ = 190 kJ/(K m²))	
Weather	M_1	M_2	M_1	M_2
C_1	**4.53[4.41; 4.70]**	**4.82[4.34; 5.08]**	**171[151; 211]**	**195[158; 796]**
C_2	4.50[4.42; 4.59]	4.42[4.18; 4.77]	181[143; 383]	210[159; 765]
C_3	4.42[4.30; 4.54]	4.88[4.75; 5.04]	173[147; 205]	721[468; 816]
C_4	4.41[4.19; 4.76]	4.49[4.30; 4.75]	188[137; 749]	286[149; 667]
C_5	5.23[4.73; 5.70]	5.53[4.63; 6.78]	189[163; 772]	673[229; 826]
C_6	5.10[4.92; 7.14]	6.37[4.46; 11.97]	199[138; 769]	288[199; 816]

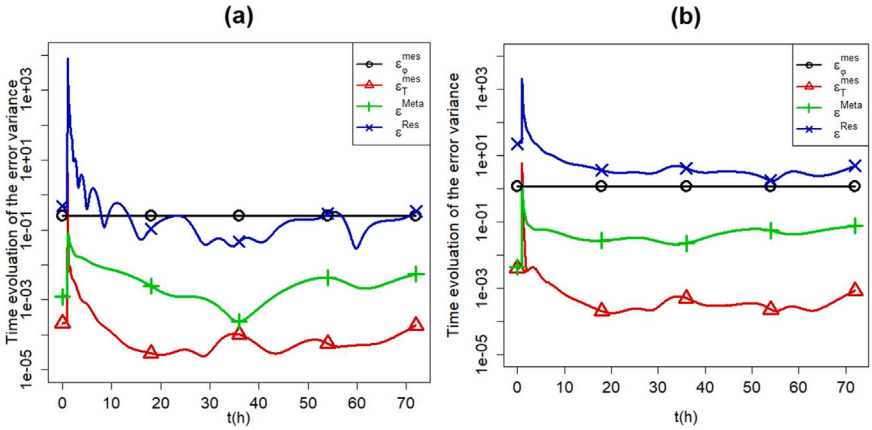

Fig. 10. Time evolution of the error variance of each uncertainty quantified (see Section 3) in the case of weather M_1 and configuration C_2 for the walls W_2 (a) and W_4 (b).

approximation of the imposed temperatures.[1] In addition, the variance error associated with the replacement of the 1D model by its meta-model (ε^{Meta}) is much smaller than the error of the flux measurements, which is constant during the whole measurement. Finally, we see that in the case of W_2, the largest (by far) contributor to the global error is the residual error during the first 10 h of the study. This error becomes of the same order as the flux measurement error ($\varepsilon_{\varphi}^{mes}$) after 10 h. These conclusions are different when focusing on wall W_4. In this case ε^{Res} is large compared to the other error terms during the whole experiment. This can be attributed to the higher modelling error between the 3D and the 1D model when e_{Tot} increases [7]. So, in the case of very thick walls under localised active solicitation, it is preferable exploring the meta-modelling of the 3D model instead of the 1D one.

To better quantify the amplitude of each error term, Table 8 also provides the variances of these errors averaged over the measurement time for configuration C_2. It confirms that the residual error (ε^{Res}) is the greatest for the two considered weathers and the four walls tested. As already mentioned in Section 4.1.2, a reduction in the number of parameters based on a sensitivity analysis is applied when creating the meta-model. In the case of W_1 where the total thickness of the wall is very small (e_{Tot} = 0.21 m) the parameters of outside layers 3 and 4 can have an influence on φ_{S_i}. However, in order to construct the predictors in a similar way for the different walls, only 5 parameters are used to create the φ_{S_i} predictor for W_1, which introduces a source of uncertainty that makes the ε^{Res} large. On the other hand, we observe that during the first 10 h of excitation, the residual error is very large, which may be related to time discretisation error due to the sharp variation of φ_{S_i} resulting from the excitation on the inner surface (see Fig. 6). After reaching a stable form of φ_{S_i}, the residual error stabilises and becomes larger in the case of W_4 (compared to the cases of W_2 and W_3). This phenomenon could be due to the difference between the 3D model and the simplified 1D model used (modelling error), which increases with greater thicknesses.

[1] It should be emphasised that this error term does not directly reflect the influence of measurement uncertainties on the imposed temperatures, but rather the influence of the error residual potentially still present after smoothing.

Table 8
Mean on time of the error variance of each uncertainty quantified (see Section 3) in W m^{-2} : $\varepsilon_{\varphi}^{\text{mes}}$ as $\bar{V}_{\varphi}^{\text{mes}}$, $\varepsilon_{\text{T}}^{\text{mes}}$ as $\bar{V}_{\text{T}}^{\text{mes}}$, $\varepsilon^{\text{Meta}}$ as $\bar{V}^{\text{Meta}}$, ε^{Res} during the first 10 h of excitation as $\bar{V}_1^{\text{Res}}$, ε^{Res} after the first 10 h of excitation as $\bar{V}_2^{\text{Res}}$. They are calculated in the case of weathers M_1 and M_2 and configuration C_2 (φ_{S_i} only) for the walls studied.

Weather	M_1					M_2				
Error	$\bar{V}_{\varphi}^{\text{mes}}$	$\bar{V}_{\text{T}}^{\text{mes}}$	$\bar{V}^{\text{Meta}}$	$\bar{V}_1^{\text{Res}}$	$\bar{V}_2^{\text{Res}}$	$\bar{V}_{\varphi}^{\text{mes}}$	$\bar{V}_{\text{T}}^{\text{mes}}$	$\bar{V}^{\text{Meta}}$	$\bar{V}_1^{\text{Res}}$	$\bar{V}_2^{\text{Res}}$
W_1	0.22	0.001	0.08	209	19.6	0.22	0.0006	0.32	103	7.28
W_2	0.25	0.002	0.004	79.0	0.16	0.25	0.0006	0.11	22.6	0.04
W_3	0.25	0.004	0.06	6.58	0.60	0.25	0.004	0.002	1.07	0.001
W_4	1.18	0.005	0.04	44.0	3.37	1.17	0.004	0.09	827	2.43

Table 9
Description of the real internal insulation wall: geometry and measured thermophysical properties of materials - Total wall thermal resistance deduced from measured material properties $R_{\text{Tot}}^{th} = 4.02$ m^2 K/W.

Layer	Material	e (m)	λ (W/(m K))
1	Plasterboard	0.013	0.25
2	Expanded polystyrene	0.12	0.032
3	Building block	0.15	0.74
4	External coating	0.015	0.94

Fig. 11. Tested internal insulation wall — construction phase: mounting of building blocks (a), adding insulation and plasterboard (b) and identification test phase at Cerema Nancy: view of the outside wall face, with a sun cover, exposed to natural conditions (c).

4.2. On measured data for IIW

The identification method presented in Section 3 is now applied to a real wall in natural weather conditions [8]. It corresponds to an internal insulation wall (IIW) of total thickness $e_{\text{Tot}} = 0.298$ m with 4 layers. The description of the wall and the measured material thermal properties by means of guarded hot plate or hot disk are summarised in Table 9. The theoretical wall resistance $R_{\text{Tot}}^{\text{th}}$ calculated from material thermal properties corresponds to 4.02 m^2 K/W. This IIW of dimension 2×2 m^2, represented in Fig. 11, was specifically built in the research project RESBATI to be transportable to different sites to conduct different types of tests. Indeed, a reference total thermal resistance of the wall of 3.5 ± 0.8 m^2 K/W was first determined in laboratory using guarded hot box at CSTB, France. Then, the real IIW, denoted "W5" in the following, was moved to the Cerema at Nancy (France) and was tested using a developed lamp box prototype under natural weather conditions for *in-situ* wall thermal resistance determination [8]. Its external surface was exposed to the sun and external temperature variations. During the test, sensors were placed on the inner and outer surfaces of the wall to measure T_{S_i}, T_{S_e} and variations in φ_{S_i}. To evaluate the identification method in an operational context, there was no measurements of the heat flux on exterior wall face and no stabilisation phase. The measurement and excitation of the inner wall surface, by imposing a Φ_{exc} of approximately 240 W/m^2, were conducted on a reduced time of 10 h. This test is denoted $M_{2bis}C_6W_5$. The weather M_{2bis} is associated with the measured climatic conditions at Nancy (France) in August 2020 where outdoor temperatures ranged from 16°C to 30°C and solar irradiance from 0 W/m^2 to 622 W/m^2 respectively during the considered 10 h test period.

Before presenting the results of the identification of the thermal resistance using real data (see Section 4.2.2), a numerical study is carried out in the next section on this wall W_5, considering M_2 weather, to get a better understanding of expected identification results using a reduced instrumentation and short measurement time.

4.2.1. Numerical test

To mimic the experimental case corresponding to the available measurements, numerical tests for different configurations on W_5, with M_2 weather and a controlled excitation Φ_{exc} of 240 W/m^{2}on the inside wall face, are tested and presented in Table 10. It can be seen that in the tests $M_2C_1W_5$ and $M_2C_2W_5$, R_{Tot} is identified with very high accuracy and low uncertainty. In the case of test $M_2C_5W_5$ with a reduced 10 h excitation time, the identification of R_{Tot} is proper but with a higher uncertainty, which is still

Table 10
Numerical identification of the resistance of each layer (R_i) and R_{Tot} (in m^2 K/W) of the wall W_5 in the case of the M_2 weather, in the configurations C_1, C_2, C_5 and C_6. The results of the estimation of the thermal resistance are presented in the form MAP[$IC_{95\%}$] where MAP is the value which maximises the *a posteriori* distribution and [$IC_{95\%}$] is the confidence interval at 95%.

Test	R^{Ref}	$M_2C_1W_5$	$M_2C_2W_5$	$M_2C_5W_5$	$M_2C_6W_5$
R_1	0.05	0.04[0.02; 0.08]	0.04[0.04; 0.05]	0.05[0.04; 0.06]	0.05[0.04; 0.05]
R_2	3.87	3.31[3.14; 3.43]	3.62[3.33; 3.89]	3.11[2.76; 3.61]	3.02[2.75; 3.48]
R_3	0.20	0.72[0.61; 0.87]	0.14[0.07; 0.60]	1.44[0.74; 2.18]	2.50[0.30; 2.93]
R_4	0.01	0.03[0.01; 0.05]	0.04[0.01; 0.29]	0.03[0.009; 0.28]	0.02[0.009; 0.29]
R_{Tot}	**4.13**	**4.12[4.00; 4.22]**	**4.06[3.95; 4.20]**	**4.70[4.27; 5.34]**	**5.61[3.73; 6.25]**

Table 11
Experimental identification on *in-situ* interior insulation wall at Cerema Nancy exposed to natural summer conditions. The results of the estimation of the thermal resistance (R^{Est}) are presented in the form MAP[$IC_{95\%}$] where MAP is the value which maximises the a posteriori distribution and [$IC_{95\%}$] is the credible interval at 95%. R^{th} correspond to the theoretical values deduced from measured material properties and considered as the reference values.

	R_1	R_2	R_3	R_4	R_{Tot}
R^{th}	0.05	3.75	0.20	0.01	**4.02**
R^{Est}	0.14[0.09; 0.14]	3.65[3.39; 4.02]	2.61[0.17; 2.93]	0.04[0.01; 0.29]	**6.42[4.24; 6.86]**

acceptable. In the case of the last test performed $M_2C_6W_5$ whose configuration corresponds to the available experimental data (see Section 4.2.2), R_{Tot} is identified with larger uncertainty, while retaining the information that the wall has a resistance greater than 3.58 m^2 K/W ($R_{Tot} \geq 3.73$ m^2 K/W). We note that the measurement of the φ_{S_e} improves the identification of R_{Tot} in the case of an IIW wall with a reduced excitation time (10 h) and an imposed Φ_{exc} of 240 W/m^2. We conclude that, for this wall W_5 with the thermal properties given in Table 9, a 10-hour excitation of 240 W/m^2 for the inner surface, using temperature and flux sensors of the inner and outer surfaces, allows to identify the total thermal resistance of the wall with accuracy and with acceptable uncertainties. If the information on the minimum total resistance of the wall and the resistance of the insulation is sufficient, it is thus enough to excite the inner surface for 10 h and to measure only T_{S_i}, T_{S_e} and φ_{S_i}.

4.2.2. Experimental test

After the numerical study of the different tests presented in Table 10, in this section we present the experimental application on a real IIW with real sensor outputs. As explained before, the IIW was placed and tested at Cerema in Nancy (France) during the summer 2020. The inside wall face (resp. outside wall face) was in contact with a controlled indoor environment at a 20°C fixed temperature (resp. the external natural environment, which enables solar radiation). To estimate the overall wall thermal resistance in a short measurement time (10 h) while limiting the influence of outside weather conditions: (i) an active solicitation of about 240 W/m^2 on a 60 cm × 60 cm area of the inside wall face was ensured by a developed prototype [8] equipped with halogen spots, (ii) a (60 cm × 60 cm) solar protection was placed on the measurement zone of the outside wall surface to reduce the impact of solar radiation. During the test, the outdoor temperature was between 16°C and 30°C and the solar irradiance was between 0 W/m^2 and 622 W/m^2. For operational purposes, we recall that temperature sensors were placed on both wall sides (T_{S_i} and T_{S_e}) whereas a heat flux sensor was only placed on the inside surface (φ_{S_i}). The considered test, denoted "Test 21" in [8], was conducted in August 2020 during the daytime. The values of measurement uncertainties used in the Bayesian identification process are similar to those defined in the numerical study in Section 4.1, and are in agreement with the instrumentation deployed. The data available presented in Fig. 12 correspond to measurements with only 10 h of excitation of the inner surface by imposing a Φ_{exc} of approximately 240 W/m^2 and without a stabilisation phase. It shows a comparison between the variation of the T_{S_i} and T_{S_e} and their smoothed versions (a) and the variation of the φ_{S_i} (b).

Given the data available (see Fig. 12), we are in the case $M_{2bis}C_6W_5$. As shown in Table 11, given the short duration of the excitation (10 h) and the fact that limited instrumentation was used (no sensors to measure the heat flux on the external surface), we do not have enough information to identify the resistances of layers 3 (building block) and 4 (external coating). Fig. 13 shows the total thermal resistance deduced from measured material properties ($R^{th}_{Tot} = 4.02$ m^2 K/W), the *a posteriori* distribution of the estimated R_{Tot} (in brown), the value that maximises the likelihood (in red, MAP = 6.42 m^2 K/W), and the credible interval of level 95% (in blue, $CI_{95\%} = [4.24; 6.86]$). We obtained a perfect estimate of the thermal resistance of the insulation (R_2) with a high degree of accuracy and we succeeded in estimating the minimum thermal resistance of the entire wall W_5 (R_{Tot}) correctly, but with significant uncertainties (wide credible intervals), as shown in the Table 11.

As demonstrated previously in the numerical case $M_2C_6W_5$ (see Table 10), the limited instrumentation and the short measurement time (10 h) leads to large uncertainties. We also note the difficult nature of this real experimental test, conducted in the summer, which does not facilitate the identification of the wall thermal resistance. It leads to higher uncertainties than the numerical cases but we identify properly the R_i minima of each layer, especially R_2 and R_{Tot}.

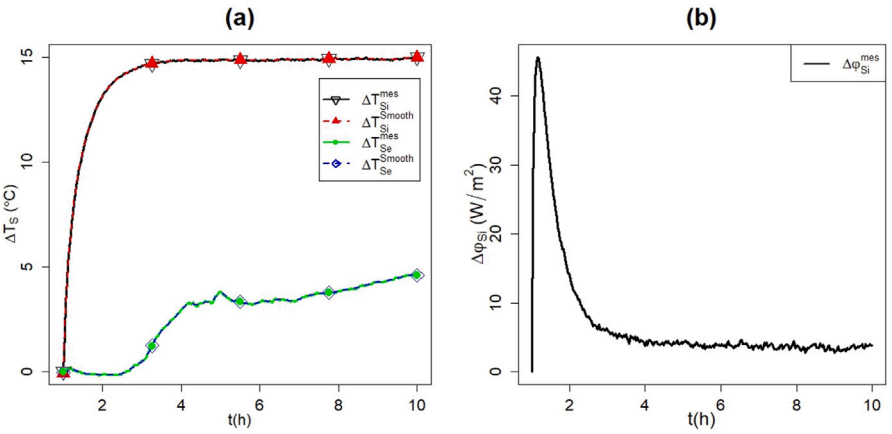

Fig. 12. Comparison of noisy and smoothed surfaces temperatures variation ΔT_S (a) and the variation of the interior surface flux $\Delta\varphi_{S_i}$ (b).

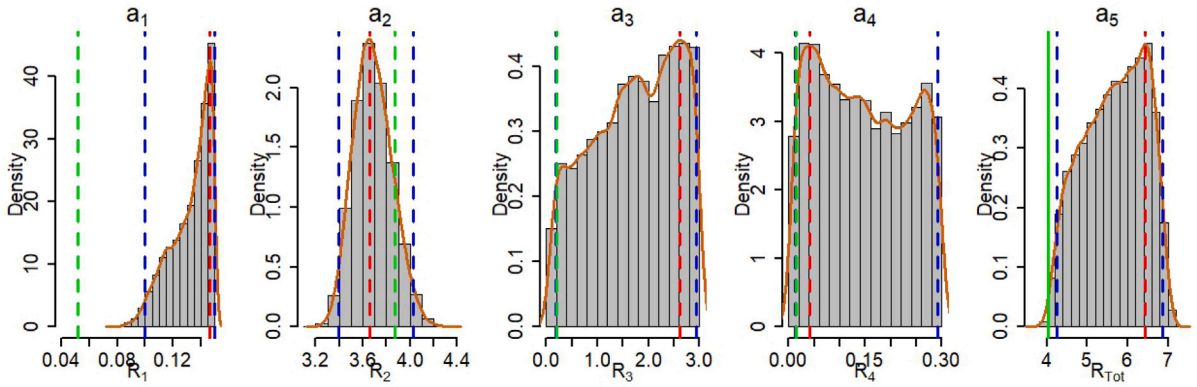

Fig. 13. A posteriori distribution of the estimated resistance (in brown), the value that maximises the likelihood (in red), the total thermal resistance value ($\boldsymbol{R}^{\mathrm{th}}_{\mathrm{Tot}}$) deduced from materials thermal characterisation (in green) and considered as the reference value, and the credible interval at 95% (in blue) for real IIW. The graph a_1 is associated with the internal coating; a_2 correspond to the insulation, a_3 refer to the support wall, a_4 characterise the external coating, and a_5 correspond to the total wall. (For interpretation of the references to colour in this figure legend, the reader is referred to the web version of this article.)

5. Conclusion and perspectives

This study presents an *in-situ* identification method for determining the total thermal resistance (R_{Tot}) for poorly insulated walls ($R_{\mathrm{Tot}} \leq 1$ m^2 K/W) as well as for highly insulated walls ($R_{\mathrm{Tot}} \geq 8$ m^2 K/W) with very different thicknesses ($0.2 < e_{\mathrm{Tot}}(\mathrm{m}) < 0.6$). It is applied in a Bayesian framework with the aim of providing a credible interval for the estimated parameters by quantifying the different sources of uncertainty. The parameter estimation is based on the Metropolis–Hastings algorithm, which requires a large number of calls to a 1D thermal model. To achieve this estimation in a reasonable computational time, a meta-model is created based on a statistical multi-fidelity approach. To reduce the influence of the initial wall temperature and the misknown heat transfer coefficients on the identification results, polynomial initial temperature profiles in the wall layers are proposed and the measured internal ($T_{\mathrm{S_i}}$) and external ($T_{\mathrm{S_e}}$) surface temperatures are imposed as boundary conditions in the thermal model. In addition, to limit the influence of external weather conditions, an active thermal solicitation on the inner surface of the wall with a Heaviside type excitation ($\boldsymbol{\Phi}_{\mathrm{exc}}$) is considered.

The proposed method is first applied to various numerical tests in two different weather conditions to study the impact of the excitation times and instrumentation on the estimation results, and thus to determine operational conditions needed for acceptable identification quality. An uncertainty analysis is performed by quantifying the different sources of error. This makes it possible to (1) control the error of the meta-model and check that it is less than the measurement error, (2) show that the reduction of model parameters in the meta-model is correct for thick walls and (3) identify the walls that require an enriched (3D) model in the multi-fidelity approach based on the residual uncertainty. The results of the numerical tests show that when the internal surface of an IIW is excited with a fixed and controlled $\boldsymbol{\Phi}_{\mathrm{exc}}$, the use of the measurement of the external surface flux allows to reduce the

uncertainties related to the estimation of R_{Tot}, especially when the internal surface is excited during only 10 h. However, a relevant estimate of the total thermal resistance can also be obtained by using only the internal surface flux when considering a longer excitation time of 3 days. It should also be noted that for some cases tested, an accurate estimation of the wall thermal capacitance is provided (which is not the main objective of this study). In addition, an *in-situ* experimental application is carried out on a real IIW in natural weather conditions, using available data from 10 h of excitation with $\Phi_{\mathrm{exc}} = 240$ W/m^2. It shows that a relevant estimation of the thermal resistance of the insulation (± 0.3 m^2 K/W) and a proper estimate of the minimum thermal resistance of the wall are provided using a reduced instrumentation and a short excitation time. Finally, we note that the method proposed in this study is not limited to the case of internally insulated walls, but can be applied to other types of wall (for example single-layer walls) and for different weather conditions.

In perspectives, a meta-model of the 3D model could be created for thick walls by adding a third level of fidelity which will reduce model errors and consequently provide more accurate estimates of R_{Tot} with less uncertainty. This improvement can be valuable for a part of internal insulated walls and also for single-walls. The proposed method and experimental protocol can also be adapted to external insulated walls, notably by applying the active thermal excitation on the exterior wall surface. Lastly, experimental applications on hygroscopic walls (i.e. bio-based and geo-sourced walls) will be conducted with the aim of identifying not only thermal but also hygrothermal properties.

CRediT authorship contribution statement

H. Nasser: Writing – review & editing, Writing – original draft, Validation, Software, Methodology, Conceptualization. **G. Perrin:** Writing – review & editing, Writing – original draft, Validation, Supervision, Software, Resources, Methodology, Conceptualization. **R. Chakir:** Writing – review & editing, Validation, Methodology, Conceptualization. **S. Demeyer:** Writing – review & editing, Validation, Methodology, Conceptualization. **J. Waeytens:** Writing – review & editing, Writing – original draft, Validation, Supervision, Software, Methodology, Funding acquisition, Conceptualization.

Declaration of competing interest

The authors declare the following financial interests/personal relationships which may be considered as potential competing interests: Julien Waeytens reports financial support was provided by French National Research Agency. If there are other authors, they declare that they have no known competing financial interests or personal relationships that could have appeared to influence the work reported in this paper.

Acknowledgements

This work, carried out as part of the "RESBIOBAT" project, was funded by the French National Research Agency (ANR) under the reference ANR-21-CE22-0018-01. The authors would also like to thank the researchers and engineers involved in the "RESBATI" project, in particular Laurent Peiffer who conducted the experiments at Cerema Nancy.

Appendix A. Details of polynomial initial condition temperature profile

A $t = t_0$, to determine the polynomial initial temperature profile, we use the temperature and heat flux measured on indoor and outdoor wall faces and also the continuity conditions at the wall layer interfaces. It gives 10 equations:

- Measurements (4 equations):

$$\begin{cases} T_1(x_1 = 0) = T_{\mathrm{S_i}}, \\ T_4(x_4 = 1) = T_{\mathrm{S_e}}, \\ \varphi_1(x_1 = 0) = \varphi_{\mathrm{S_i}}, \\ \varphi_4(x_4 = 1) = \varphi_{\mathrm{S_e}}. \end{cases} \tag{A.1}$$

- Continuity conditions (6 equations) :

$$\begin{cases} T_i(x_i = 1) = T_{i+1}(x_{i+1} = 0) \ \text{ for } i \in [1, 3], \\ \varphi_i(x_i = 1) = \varphi_{i+1}(x_{i+1} = 0) \ \text{ for } i \in [1, 3]. \end{cases} \tag{A.2}$$

The 10 polynomial coefficients involved in the proposed initial temperature profile (see Eq. (8)) are determined by solving the system:

$$\begin{cases} T_1(x_1=0) = T_{S_i} \implies b_1 = T_{S_i} \\ q_1(x_1=0) = q_{S_i} \implies a_1 = -R_1 q_{S_i} \\ T_4(x_4=1) = T_{S_e} \implies a_4 + b_4 + c_4 = T_{S_e} \\ q_4(x_4=1) = q_{S_e} \implies -\frac{2a_4+b_4}{R_4} = q_{S_e} \\ T_1(x_1=1) = T_2(x_2=0) \implies a_1 + b_1 = b_2 \\ T_2(x_2=1) = T_3(x_3=0) \implies a_2 + b_2 = c_3 \\ T_3(x_3=1) = T_4(x_4=0) \implies a_3 + b_3 + c_3 = c_4 \\ q_1(x_1=1) = q_2(x_2=0) \implies -\frac{a_1}{R_1} + \frac{a_2}{R_2} = 0 \\ q_2(x_2=1) = q_3(x_3=0) \implies -\frac{a_2}{R_2} + \frac{b_3}{R_3} = 0 \\ q_3(x_3=1) = q_4(x_4=0) \implies \frac{b_4}{R_4} - \frac{2a_3+b_3}{R_3} = 0 \end{cases} \tag{A.3}$$

We can show that the solution of the system is:

$$\begin{cases} a_1 = -R_1 q_{S_i} \\ a_2 = -R_2 q_{S_i} \\ a_3 = \frac{R_3}{2(R_3+R_4)}(2(R_1+R_2+R_3)q_{S_i} + R_4(q_{S_i}+q_{S_e}) + 2(T_{S_e} - T_{S_i})) \\ a_4 = -\frac{R_4}{2(R_3+R_4)}(2(R_1+R_2)q_{S_i} + R_3(q_{S_i}+q_{S_e}) + 2R_4 q_{S_e} + 2(T_{S_e} - T_{S_i})) \\ b_1 = T_{S_i} \\ b_2 = -R_1 q_{S_i} + T_{S_i} \\ b_3 = -R_3 q_{S_i} \\ b_4 = \frac{R_4}{R_3+R_4}(2(R_1+R_2)q_{S_i} + R_3 q_{S_i} + R_4 q_{S_e} + 2(T_{S_e} - T_{S_i})) \\ c_3 = -(R_1+R_2)q_{S_i} + T_{S_i} \\ c_4 = -\frac{1}{2(R_3+R_4)}(2R_4(R_1+R_2)q_{S_i} + R_3 R_4(q_{S_i} - q_{S_e}) - 2R_3 T_{S_e} - 2R_4 T_{S_i}) \end{cases} \tag{A.4}$$

Appendix B. Metropolis–Hastings algorithm

This section briefly presents the basics of the Metropolis Hastings (MH) algorithm used for the MCMC step. In this section, we use the same notation as in Section 3.1, but we assume that the components of $\boldsymbol{z}$ have been normalised with respect to their *a priori* distribution, in the sense that all the components of $\boldsymbol{z}$ now have zero means and variances of 1.

To begin, the HM algorithm specify a starting point $\boldsymbol{z}^0$ (which can be done randomly) and a proposal probability distribution q. In this work, we limit ourselves to the following Gaussian proposal parameterised by a unique scale parameter ω (if the components of $\boldsymbol{z}$ were not normalised, this proposal distribution would have to take account of potential differences in the order of magnitude between the components of $\boldsymbol{z}$, potentially by depending on a larger number of hyper-parameters) :

$$q(\boldsymbol{z}^1|\boldsymbol{z}^2) = \frac{1}{\omega^8(2\pi)^4}\exp\left(-\frac{\left\|\boldsymbol{z}^1 - \boldsymbol{z}^2\right\|^2}{2\omega^2}\right), \quad \boldsymbol{z}^1, \boldsymbol{z}^2 \in \mathbb{R}^8. \tag{B.1}$$

The MH algorithm then sequentially adds new samples to the chain in two steps: a new sample $\boldsymbol{z}^*$ is proposed at iteration n based on the previous sample $\boldsymbol{z}^{n-1}$, and this proposed sample is either added to the chain (in this case $\boldsymbol{z}^n = \boldsymbol{z}^*$) or rejected with some probability (in that case, $\boldsymbol{z}^n = \boldsymbol{z}^{n-1}$). The probability of acceptance is generally chosen equal to

$$\beta = \min\left[1, \frac{\pi(\boldsymbol{z}^*|\boldsymbol{y}^{\text{mes}}) \times q(\boldsymbol{z}^{n-1}|\boldsymbol{z}^*)}{\pi(\boldsymbol{z}^{n-1}|\boldsymbol{y}^{\text{mes}}) \times q(\boldsymbol{z}^*|\boldsymbol{z}^{n-1})}\right]. \tag{B.2}$$

After N_s iterations, we obtain a sequence $\{\boldsymbol{z}^1, \dots, \boldsymbol{z}^{N_s}\}$ that can be used to approximate the posterior distribution $\pi(\boldsymbol{z}|\boldsymbol{y}^{\text{mes}})$.

The choice of ω is central to such an algorithm. See [53] for more details on this choice of ω and its potential adaptation as a function of n.

Appendix C. Gaussian smoothing

We are interested here in the approximation of a function $t \mapsto y(t)$ that is observed in N points $t_1, \dots, t_N$. Let $\boldsymbol{y}^{\text{mes}} = (y^{\text{mes}}(t_1), \dots, y^{\text{mes}}(t_N))$ be the vector gathering these N observations. It is assumed that these N measurements are all affected by the same Gaussian noise, and that these noises are mutually independent. Let σ^2 be the variance of this noise. Assume now that $t \mapsto y(t)$ is a particular realisation of a Gaussian process $t \mapsto Y(t)$ with mean function $t \mapsto m(t)$ and covariance function $(t, t') \mapsto k(t, t')$, which is assumed independent of the noise. For all t, we deduce that:

Algorithm 1: MCMC Algorithm

Define the starting point $\boldsymbol{z}^0$, the proposal distribution q, and the scale parameter ω ;
Set state indicator $n = 1$;
Compute $\pi(\mathbf{z}^{n-1}|\mathbf{y}^{\text{mes}})$;
while $n < N_s$ **do**
  Sample at random a candidate point $\boldsymbol{z}^*$ according to PDF $q(\cdot|\boldsymbol{z}^{n-1})$;
  Compute $\pi(\mathbf{z}^*|\mathbf{y}^{\text{mes}})$ and acceptance factor β with Eq. (B.2) ;
  Draw at random and uniformly between 0 and 1 the value U ;
  if $U \leq \beta$ **then**
    $\boldsymbol{z}^n = \boldsymbol{z}^*$;
  else
    $\boldsymbol{z}^n = \boldsymbol{z}^{n-1}$;
  $n = n + 1$;

$$\begin{pmatrix} Y(t) \\ \boldsymbol{y}^{\text{mes}} \end{pmatrix} \sim \mathcal{N}\left(\begin{pmatrix} m(t) \\ \boldsymbol{m} \end{pmatrix}, \begin{bmatrix} k(t,t) & \boldsymbol{r}^T(t) \\ \boldsymbol{r}(t) & \sigma^2 \boldsymbol{I}_N + \boldsymbol{K} \end{bmatrix}\right), \tag{C.1}$$

$$\boldsymbol{m} = \begin{pmatrix} m(t_1) \\ \vdots \\ m(t_N) \end{pmatrix}, \quad \boldsymbol{K} = \begin{bmatrix} k(t_1,t_1) & \cdots & k(t_1,t_N) \\ \vdots & \ddots & \vdots \\ k(t_N,t_1) & \cdots & k(t_N,t_N) \end{bmatrix}, \tag{C.2}$$

By stability of the Gaussian distribution through conditioning [49], it comes:

$$Y(t) \mid \boldsymbol{y}^{\text{mes}} \sim \text{GP}\begin{pmatrix} t \mapsto m(t) + \boldsymbol{r}^T(t)\left(\sigma^2 \boldsymbol{I}_N + \boldsymbol{K}\right)^{-1}\left(\boldsymbol{y}^{\text{mes}} - \boldsymbol{m}\right), \\ (t,t') \mapsto k(t,t') - \boldsymbol{r}^T(t)\left(\sigma^2 \boldsymbol{I}_N + \boldsymbol{K}\right)^{-1}\boldsymbol{r}(t') \end{pmatrix}. \tag{C.3}$$

Considering a smooth mean function and a smooth covariance function for Y (take, for example, the square exponential kernel $k(t,t') = \exp(-(t-t')^2/\ell^2)$ with ℓ a scaling parameter to be adjusted to the data), the function $t \mapsto m(t) + \boldsymbol{r}^T(t)\left(\sigma^2 \boldsymbol{I}_N + \boldsymbol{K}\right)^{-1}(\boldsymbol{y}^{\text{mes}} - \boldsymbol{m})$ provides a smoothed approximation of $t \mapsto y(t)$. By generating independent realisations of $t \mapsto Y(t) \mid \boldsymbol{y}^{\text{mes}}$, we also generate smooth approximations of y which are themselves fully consistent with the available data contained in $\boldsymbol{y}^{\text{mes}}$.

In absolute terms, we can take $m(t) = 0$ for all t. However, if we consider stationary covariance functions for Y (as it is almost always the case), it is worth looking for mean functions m that make the function $t \mapsto Y(t) - m(t)$ as stationary as possible.

Appendix D. R5C4 thermal model and relations between RC and 1D model parameters

The considered RC model is defined by 5 resistances and 4 capacitance. It is denoted as R5C4. To determine the 4 wall nodal temperatures $(T_{m_1}, T_{m_2}, T_{m_3}, T_{m_4})$, we need to solve the system defined below for $t \in [t_0, t_f]$ where the surface temperatures (T_{S_i}, T_{S_e}) are used as boundary conditions (see Section 2.2):

$$C\frac{\partial T_{RC}}{\partial t} + KT_{RC} = F, \tag{D.1}$$

where

$$T_{RC} = (T_{m_1}, T_{m_2}, T_{m_3}, T_{m_4}), \; F = \left(\frac{T_{S_i}}{R_A}, 0, 0, \frac{T_{S_e}}{R_E}\right), \tag{D.2}$$

$$K = \begin{pmatrix} \frac{1}{R_A} + \frac{1}{R_B} & -\frac{1}{R_B} & 0 & 0 \\ -\frac{1}{R_B} & \frac{1}{R_B} + \frac{1}{R_C} & -\frac{1}{R_C} & 0 \\ 0 & -\frac{1}{R_C} & \frac{1}{R_C} + \frac{1}{R_D} & -\frac{1}{R_D} \\ 0 & 0 & -\frac{1}{R_D} & \frac{1}{R_D} + \frac{1}{R_E} \end{pmatrix}, \; C = \begin{pmatrix} C_1 & 0 & 0 & 0 \\ 0 & C_2 & 0 & 0 \\ 0 & 0 & C_3 & 0 \\ 0 & 0 & 0 & C_4 \end{pmatrix}. \tag{D.3}$$

According to Eq. (23), the mean function of the meta-model created is chosen as an estimated constant α multiplied by the numerical solution of the RC model. Since the input parameters of the meta-model correspond to the parameters of the 1D model represented by the vector $\boldsymbol{z}$ (see Section 2.5), the relations between the RC and 1D model parameters are:

$$\begin{cases} R_A = \frac{R_1}{2}, \; R_B = \frac{R_1}{2} + \frac{R_2}{2}, \; R_C = \frac{R_2}{2} + \frac{R_3}{2}, \; R_D = \frac{R_3}{2} + \frac{R_4}{2}, \; R_E = \frac{R_4}{2}, \\ C_i = e\rho C_i \text{ for } i \in [1,4]. \end{cases} \tag{D.4}$$

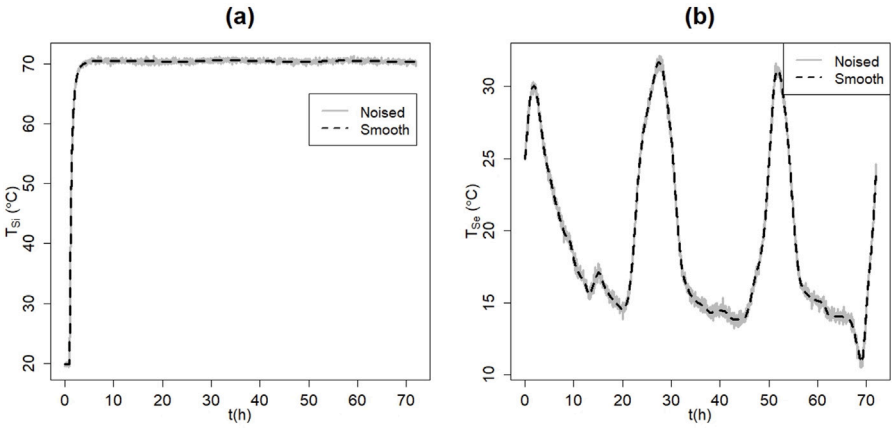

Fig. E.14. Comparison of noisy and smoothed temperatures in the case of Carpentras, wall 2: (a) T_{S_i}, (b) T_{S_e}.

Appendix E. Smoothing of measured temperatures

In Fig. E.14, a comparison between the noisy measurements (in grey) and their smoothed versions (in black) is shown for T_{S_i} and T_{S_e} in the case of Carpentras, for wall "W_2". Given the particular form of T_{S_i}, a parametric mean function m (see Appendix C for more details) is chosen for the rise of T_{S_i} so that

$$m(t) = T_{S_i}(t = t_0) + B_1 \left(1 - \exp\left(\frac{-B_2(t - t_0)}{t_f - t_0}\right)\right), \quad t \in [t_0, t_f], \tag{E.1}$$

where B_1, B_2 are estimated using a least-squares procedure.

Data availability

Data will be made available on request.

References

[1] John Conti, Paul Holtberg, Jim Diefenderfer, Angelina LaRose, James T Turnure, Lynn Westfall, International energy outlook 2016 with projections to 2040, USDOE Energy Information Administration (EIA), Washington, DC (United States, 2016.
[2] GlobalABC (Global Alliance for Buildings and Construction), IEA (International Energy Agency), UNEP (the United Nations Environment Programme), GlobalABC Roadmap for Buildings and Construction: Towards a Zero-Emission, Efficient and Resilient Buildings and Construction Sector, IEA Paris, France, 2020.
[3] Lea Gynther, Bruno Lappillone, Karine Pollier, Energy efficiency trends and policies in the household and tertiary sectors, in: An Analysis Based on the ODYSSEE and MURE Databases, vol. 97, European Union Brussels, Belgium, 2015.
[4] Réglementation Thermique RT 2005, Ed. Centre scientifique et technique du bâtiment, 2005, (in French).
[5] Réglementation Thermique RT 2012, Ed. Centre scientifique et technique du bâtiment, 2012, (in French).
[6] Réglementation environnementale RE2020, Ed. Centre scientifique et technique du bâtiment, 2020, (in French).
[7] T. Ha, V. Feuillet, J. Waeytens, K. Zibouche, S. Thebault, R. Bouchie, V. Le Sant, L. Ibos, Benchmark of identification methods for the estimation of building wall thermal resistance using active method: Numerical study for IWI and single-wall structures, Energy Build. 224 (2020) 110130.
[8] Thanh-Tung Ha, Vincent Feuillet, Julien Waeytens, Kamel Zibouche, Laurent Peiffer, Yann Garcia, Véronique Le Sant, Rémi Bouchie, Alain Koenen, Jean-Pierre Monchau, et al., Measurement prototype for fast estimation of building wall thermal resistance under controlled and natural environmental conditions, Energy Build. 268 (2022) 112166.
[9] Emilio Sassine, Yassine Cherif, Emmanuel Antczak, Joseph Dgheim, Thermal characterization of building walls under random boundary conditions, J. Therm. Sci. Eng. Appl. 13 (5) (2021) 054502.
[10] ISO ISO, 9869-1: 2014 Thermal Insulation, Building Elements, In-Situ Measurement of Thermal Resistance and Thermal Transmittance-Part 1: Heat Flow Meter Method, BSI, London, 2014.
[11] Arash Rasooli, Laure Itard, In-situ characterization of walls' thermal resistance: An extension to the ISO 9869 standard method, Energy Build. 179 (2018) 374–383.
[12] Chayan Kumar Basak, Gautam Sarkar, Subhasis Neogi, Performance evaluation of material and comparison of different temperature control strategies of a guarded hot box U-value test facility, Energy Build. 105 (2015) 258–262.
[13] I. Naveros, M.J. Jiménez, M.R. Heras, Analysis of capabilities and limitations of the regression method based in averages, applied to the estimation of the U value of building component tested in mediterranean weather, Energy Build. 55 (2012) 854–872.
[14] Pier Giorgio Cesaratto, Michele De Carli, A measuring campaign of thermal conductance in situ and possible impacts on net energy demand in buildings, Energy Build. 59 (2013) 29–36.
[15] David Bienvenido-Huertas, Juan Moyano, Carlos E Rodríguez-Jiménez, David Marín, Applying an artificial neural network to assess thermal transmittance in walls by means of the thermometric method, Appl. Energy 233 (2019) 1–14.

[16] EN ISO, 8990, thermal insulation, in: Determination of Steady-State Thermal Transmission Properties–Calibrated and Guarded Hot Box, European Committee for Standardization, Brussels, Belgium, 1996.
[17] ISO ISO, 9869-2: 2018—Thermal Insulation—Building Elements—In-Situ Measurement of Thermal Resistance and Thermal Transmittance—Part 2: Infrared Method for Frame Structure Dwelling, ISO, Geneva, Switzerland, 2018.
[18] An-Heleen Deconinck, Staf Roels, Comparison of characterisation methods determining the thermal resistance of building components from onsite measurements, Energy Build. 130 (2016) 309–320.
[19] Ente Italiano di Normazione, UNI EN ISO 13786 thermal performance of building components. dynamic thermal characteristics, Calc. Methods (2008).
[20] Roberto Ricciu, Francesco Ragnedda, Alessandra Galatioto, Stefano Gana, Luigi A Besalduch, Andrea Frattolillo, Thermal properties of building walls: Indirect estimation using the inverse method with a harmonic approach, Energy Build. 187 (2019) 257–268.
[21] Zorana Petojević, Radovan Gospavić, Goran Todorović, Estimation of thermal impulse response of a multi-layer building wall through in-situ experimental measurements in a dynamic regime with applications, Appl. Energy 228 (2018) 468–486.
[22] Adrien François, Laurent Ibos, Vincent Feuillet, Johann Meulemans, Estimation of the thermal resistance of a building wall with inverse techniques based on rapid active in situ measurements and white-box or ARX black-box models, Energy Build. 226 (2020) 110346.
[23] Kenneth Levenberg, A method for the solution of certain non-linear problems in least squares, Q. Appl. Math. 2 (2) (1944) 164–168.
[24] Jorge J. Moré, The Levenberg-Marquardt algorithm: implementation and theory, in: Numerical Analysis: Proceedings of the Biennial Conference Held At Dundee, June 28–July 1, 1977, Springer, 2006, pp. 105–116.
[25] Emilio Sassine, Zohir Younsi, Yassine Cherif, Alexis Chauchois, Emmanuel Antczak, Experimental determination of thermal properties of brick wall for existing construction in the north of France, J. Build. Eng. 14 (2017) 15–23.
[26] Emilio Sassine, Yassine Cherif, Emmanuel Antczak, Parametric identification of thermophysical properties in masonry walls of buildings, J. Build. Eng. 25 (2019) 100801.
[27] Mihaela Teni, Hrvoje Krstić, Piotr Kosiński, Review and comparison of current experimental approaches for in-situ measurements of building walls thermal transmittance, Energy Build. 203 (2019) 109417.
[28] David Bienvenido-Huertas, Juan Moyano, David Marín, Rafael Fresco-Contreras, Review of in situ methods for assessing the thermal transmittance of walls, Renew. Sustain. Energy Rev. 102 (2019) 356–371.
[29] Yingying Yang, Zhoulin Chen, Tingting Vogt Wu, Alain Sempey, Jean-Christophe Batsale, In situ methodology for thermal performance evaluation of building wall: A review, Int. J. Therm. Sci. 181 (2022) 107687.
[30] Phillip Biddulph, Virginia Gori, Clifford A Elwell, Cameron Scott, Caroline Rye, Robert Lowe, Tadj Oreszczyn, Inferring the thermal resistance and effective thermal mass of a wall using frequent temperature and heat flux measurements, Energy Build. 78 (2014) 10–16.
[31] Virginia Gori, Clifford A. Elwell, Estimation of thermophysical properties from in-situ measurements in all seasons: Quantifying and reducing errors using dynamic grey-box methods, Energy Build. 167 (2018) 290–300.
[32] Lia De Simon, Marco Iglesias, Benjamin Jones, Christopher Wood, Quantifying uncertainty in thermophysical properties of walls by means of Bayesian inversion, Energy Build. 177 (2018) 220–245.
[33] Séverine Demeyer, V Le Sant, A Koenen, N Fischer, Julien Waeytens, Rémi Bouchié, Bayesian uncertainty analysis of inversion models applied to the inference of thermal properties of walls, Energy Build. 249 (2021) 111188.
[34] Julien Berger, Helcio RB Orlande, Nathan Mendes, Sihem Guernouti, Bayesian inference for estimating thermal properties of a historic building wall, Build. Environ. 106 (2016) 327–339.
[35] Julien Berger, Clemence Legros, Surface transfer coefficients estimation for heat conduction problem using the Bayesian framework, Heat Transf. Eng. 44 (5) (2023) 391–410.
[36] J.W. Baughn, J.E. Mayhew, M.R. Anderson, R.J. Butler, A Periodic Transient Method Using Liquid Crystals for the Measurement of Local Heat Transfer Coefficients, J. Heat Transfer 120 (3) (1998) 772–777.
[37] D. Naylor, Recent developments in the measurement of convective heat transfer rates by laser interferometry, Int. J. Heat Fluid Flow 24 (3) (2003) 345–355.
[38] Mehdi Bazargani, Farshad Kowsary, Methodology for estimation of local convective heat transfer coefficient for vapor condensation, Heat Transf. Eng. 36 (9) (2015) 820–828.
[39] C. Roulet, J. Gass, I. Marcus, In-situ U-value measurement: reliable results in shorter time by dynamic interpretation of measured data, ASHRAE Trans. 108 (2) (1987) 1371–1379.
[40] J.P. Kaipio, C. Fox, The Bayesian framework for inverse problems in heat transfer, Heat Transf. Eng. 32 (9) (2011) 718–753.
[41] Christian P. Robert, et al., The Bayesian Choice: from Decision-Theoretic Foundations to Computational Implementation, vol. 2, Springer, 2007.
[42] J. Andrés Christen, Colin Fox, Markov chain Monte Carlo using an approximation, J. Comput. Graph. Stat. 14 (4) (2005) 795–810.
[43] Dani Gamerman, Hedibert F. Lopes, Markov Chain Monte Carlo: Stochastic Simulation for Bayesian Inference, CRC Press, 2006.
[44] Nicholas Metropolis, Arianna W Rosenbluth, Marshall N Rosenbluth, Augusta H Teller, Edward Teller, Equation of state calculations by fast computing machines, J. Chem. Phys. 21 (6) (1953) 1087–1092.
[45] W.K. Hastings, Monte Carlo sampling methods using Markov chains and their applications, Biometrika 57 (1) (1970) 97–109.
[46] G. Perrin, C. Soize, N. Ouhbi, Data-driven kernel representations for sampling with an unknown block dependence structure under correlation constraints, J. Comput. Stat. Data Anal. 119 (2018) 139–154.
[47] G. Perrin, C. Cannamela, A repulsion-based method for the definition and the enrichment of optimized space filling designs in constrained input spaces, J. Soc. Française Stat. 158 (1) (2017) 37–67.
[48] J. Sacks, W. Welch, T. Mitchell, H. Wynn, Design and analysis of computer experiments, Statist. Sci. 4 (1989) 409–435.
[49] T.J. Santner, B.J. Williams, W.I. Notz, The Design and Analysis of Computer Experiments, Springer, New York, 2003.
[50] Stefano Conti, Anthony O'Hagan, Bayesian emulation of complex multi-output and dynamic computer models, J. Statist. Plann. Inference 140 (3) (2010) 640–651.
[51] G. Perrin, Adaptive calibration of a computer code with time-series output, Reliab. Eng. Syst. Saf. 196 (2020) 106728.
[52] Ilya M. Sobol, Global sensitivity indices for nonlinear mathematical models and their Monte Carlo estimates, Math. Comput. Simul. 55 (1–3) (2001) 271–280.
[53] Reuven Y. Rubinstein, Dirk P. Kroese, Simulation and the Monte Carlo Method, John Wiley & Sons, 2016.